



# An improved semi-active structural control combining optimized fuzzy controller with inverse modeling technique of MR damper

Pei Pei<sup>1,2</sup> · Yongbo Peng<sup>1,3,4</sup> · Canxing Qiu<sup>4</sup>

Received: 21 February 2022 / Revised: 20 July 2022 / Accepted: 15 August 2022 / Published online: 15 September 2022  
© The Author(s), under exclusive licence to Springer-Verlag GmbH Germany, part of Springer Nature 2022

## Abstract

An effective and robust semi-active control scheme using MR damper for mitigating the earthquake-induced structural responses is proposed in this study. In the first place, a human-designed fuzzy logic controller is developed, in which the uniformly distributed membership functions are adopted for both input and output variables, and the fuzzy rules are formulated based on the law of the fundamental vibration mode. Next, an inverse modeling technique is developed for identifying the input current of MR damper based on the modified Bingham-plastic model. To simultaneously mitigate the seismic responses and guide the MR damper selection, the multiobjective NSGA-II-based approach is applied. The human-designed fuzzy logic controller is then optimized, in which the parameters in the output variable range, membership functions, and the rule base are defined as the design variables. By taking into account different parameter combinations, a variety of Pareto-optimal solutions are derived, based on which the influences of the membership function's type and symmetry, as well as the rule base's symmetry on the control performance, are analyzed. Finally, the improved semi-active control systems have been constructed for both linear and nonlinear structures by combining the optimized fuzzy controller with the proposed inverse modeling technique of MR damper. Numerical results have demonstrated the effectiveness and robustness of the proposed semi-active control scheme to the uncertainties associated with structural properties and seismic excitations.

**Keywords** Fuzzy logic control · MR damper · Inverse modeling technique · Multiobjective optimization · Pareto fronts · Seismic structures

## 1 Introduction

The mitigation of destructive effects caused by natural hazards, such as strong earthquakes and high winds is of major concern in the structural engineering community. Over the

past few decades, numerous efforts have been conducted to develop versatile structural control schemes for maintaining the safety and serviceability of civil engineering structures under natural hazards (Peng and Li 2019). Structural control is usually categorized into passive, active, semi-active, and hybrid controls (Housner et al. 1997). Among these modalities, passive control has been significantly studied and applied to many engineering structures due to its simple mechanism and zero power requirement. However, the passive control cannot adapt to changing structural properties or varying loading conditions and; thus, its effectiveness is limited. Different from passive control, active control uses the external energy supplied by actuators to exert control forces on structures. Therefore, active control is usually characterized by many attractive features, such as high adaptability and large force capacity. However, active control is suffered from stability and reliability problems as well as large power consumption problems in practice. In this respect, semi-active control, which adjusts the control device's behavior by modifying the physical properties of

---

Responsible Editor: Zhen Luo

✉ Yongbo Peng  
pengyongbo@tongji.edu.cn

<sup>1</sup> State Key Laboratory of Disaster Reduction in Civil Engineering, Tongji University, Shanghai 200092, People's Republic of China

<sup>2</sup> College of Civil Engineering, Tongji University, Shanghai 200092, People's Republic of China

<sup>3</sup> Shanghai Institute of Disaster Prevention and Relief, Tongji University, Shanghai 200092, People's Republic of China

<sup>4</sup> The Key Laboratory of Urban Security and Disaster Engineering of Ministry of Education, Beijing University of Technology, Beijing 100124, People's Republic of China

embedded smart materials or mechanical systems, not only possesses the reliability of passive control and the adaptability of active control, but also has a small power requirement. Hybrid control, generally consisting of passive and active control modalities, is a feasible solution to the multilevel earthquake-resistant design of engineering structures, but it often occupies a large space. Therefore, semi-active control has drawn increasing attention from engineers and researchers in recent years.

As a kind of fail-safe device for the semi-active control system, magnetorheological (MR) damper exhibits high reliability and stability, but its inherent nonlinear hysteretic nature has brought many difficulties and challenges in the design of control strategy (Zhang and Peng 2020). Developing an effective and robust control strategy is of vital importance to utilize the full capacity of MR damper. In the past two decades, various control algorithms have been proposed for MR damper-based structural systems (Behboodi et al. 2021; Zhao et al. 2019). In 1996, Dyke et al. proposed a clipped-optimal control algorithm based on the acceleration feedback to alter the behavior of MR damper (Dyke et al. 1996, 1998). Later, some improved versions of the clipped-optimal control algorithm have been developed for providing more effective and efficient control (Pohoryles and Duffour 2015; Yoshida and Dyke 2004; Yuen et al. 2007). Apart from the clipped-optimal control family, many other semi-active control algorithms, such as the decentralized output feedback polynomial controller, modulated homogeneous friction algorithm, decentralized bang–bang control algorithm, and Lyapunov’s direct approach have been developed for MR damper-based structural systems (Cha et al. 2013; Dyke and Spencer 1997; Jansen and Dyke 2000). The above-mentioned algorithms are usually classified into traditional control strategy, in which a primary controller, such as the linear quadratic regulator (LQR) and Lyapunov algorithms, is used to provide reference control force for inducing a secondary controller to produce the actual control force. Therefore, the traditional control strategy relies on the accurate mathematical model associated with the dynamics of controlled structures. However, it is not easy to establish an exact model that well matches the structural dynamics, since structural properties, external loadings and measurements are usually full of nonlinearities and uncertainties (Chakraborty and Debbarma 2011; Li et al. 2010).

As an alternative to the traditional control strategy, one promising strategy, i.e., fuzzy logic control (FLC), is less sensitive to the uncertainties associated with structural dynamics, because it mainly uses linguistic instructions based on the human expertise as a basis for the control strategy. The inherent robustness and ability to accommodate uncertainty and imprecision have provided FLC a key advantage over traditional control strategies. Choi et al. developed a semi-active fuzzy control strategy for MR damper-based

structural system (Choi et al. 2004), in which the required voltage can be generated for producing a desired damper force. The MR damper system based on the FLC technique is further employed for seismic protection of base-isolated building structures (Jung et al. 2006), cable-stayed bridges (Ok et al. 2007), high-rise buildings (Bathaei et al. 2018), and offshore jacket platforms (Ghadimi and Taghikhany 2021).

Although FLC has been applied to various scenarios of controlled structures and systems, the design of fuzzy membership functions and rule base remains a challenging task, which is often subjective and time consuming. It is mainly because there are no provided routines for determining the parameters of membership functions and rule base. These parameters are usually selected based on the trial-and-error investigation of control effectiveness. To overcome this problem, some optimization-based methods have been developed to identify fuzzy rules and adjust membership functions by advanced optimization algorithms, such as genetic algorithm (GA) (Ali and Ramaswamy 2009), particle swarm optimization algorithm (Marinaki et al. 2011), and whale optimization algorithm (Azizi et al. 2019). Among these optimization algorithms, GA is the most widely used one. For example, to enhance the performance of FLC used for an MR damper-based building structure against earthquake ground motions, Yan and Zhou applied GA to tune fuzzy rules, in which the weighted multiobjective function is used to consider two objectives, i.e., minimizing the maximum structural displacement and acceleration (Yan and Zhou 2006). Dounis et al. developed an evolutionary fuzzy logic controller to modulate the input voltage of MR damper for reducing the seismic response of a base-isolated structure. In the design procedure, GA was employed to tune membership functions (Dounis et al. 2007). Aimed at attenuating the seismic responses of a base-isolated structure equipped with the FLC-driven MR damper system, Ali and Ramaswamy used GA to optimize both membership functions and rule base for obtaining an optimal fuzzy controller, in which the weighted multiobjective function is adopted to minimize bearing displacement and maintain the magnitude of base shear and floor acceleration (Ali and Ramaswamy 2008).

In the aforementioned studies, the control objectives for GA-optimized fuzzy controllers are all combined by weighting factors to form a onefold function-based criterion. However, a trial-and-error procedure may be required for selecting appropriate weighting factors. Some researchers try to solve multiobjective problems by introducing the nondominated sorting genetic algorithm (NSGA-II). This optimization algorithm not only allows several competing physical quantities to be included simultaneously in controller optimization, but also provides a set of Pareto-optimal solutions, instead of a single solution. For example, to ensure

both the safety and comfort of a MR damper-based structure, Shook et al. applied the NSGS-II scheme to optimize fuzzy logic controllers, in which four competitive objectives, i.e., peak interstory drift, peak acceleration, RMS of interstory drift and RMS of acceleration were considered in parallel (Shook et al. 2008b). Besides, the NSGS-II has also been successfully applied to optimize the FLC-driven MR damper-based control system in base-isolated structures (Kim and Roschke 2006, 2007; Mehrkian et al. 2019; Shook et al. 2008a), torsionally-responsive structures (Shook et al. 2009), adjacent buildings (Uz and Hadi 2014), nonlinear and plan-asymmetric structural systems (Zafarani et al. 2018).

It is noted that, in previous studies, the attention is mainly focused on minimizing the structural responses, and little attention has been given to the control requirement (Huang et al. 2009). In fact, imparting attention to the control requirement is not only an economical consideration, but also a safety consideration that helps to design appropriate control devices. If a structure is equipped with an unsuitable control device whose maximum control requirement is much lower than the desired level, the performance of the control system will be largely discounted in some situations of extreme hazards. For instance, the dampers deployed in a building of the Northeastern University of Technology, Japan experienced serious impact, which caused damage to the main structure during the Great East Japan earthquake due to the insufficient design of damper stroke (Peng et al. 2021a). Therefore, both structural response and control force need to be considered when optimizing fuzzy logic controllers, and meanwhile, the corresponding seismic performance of MR damper-based structures needs to be addressed.

On the other hand, membership functions and rule base are two important and indispensable parts of a complete fuzzy logic controller, which have been widely investigated in the literature. In previous studies, both the membership functions and fuzzy rules are either assumed to be symmetric or asymmetric. It is noted that asymmetric membership functions (fuzzy rules) may improve the controller's performance by introducing additional design parameters for providing more variability. In contrast, symmetric membership functions (fuzzy rules) may improve computational efficiency by largely reducing the number of design parameters. Therefore, it is necessary to explore the influence of symmetric and asymmetric parameter assumptions on the FLC performance for achieving a balance between computational efficiency and effectiveness. However, related research works are rare to see, although this topic is of guiding significance for the FLC design. Besides, the fuzzy output is usually defined as the current (voltage) by which the MR damper force can be calculated using the extended Bouc–Wen model (Spencer et al. 1997). It is worth noting that the evaluation of the extended Bouc–Wen model needs to solve differential

equations, which will complicate the optimization process and raise the computational cost. To improve the optimization efficiency, the optimization process can be simplified by directly defining the control force as the fuzzy output. In this regard, an inverse modeling technique needs to be developed for identifying the input current for MR damper based on the optimum control force calculated by the optimized fuzzy controller. Inverting a forward model of MR damper is the most direct approach to develop an inverse model for current identification. However, due to the highly nonlinear hysteretic nature, the commonly used forward MR damper models are usually composed of some complex equations, such as transcendental equation, differential equation, and power function, which makes it difficult to derive a direct inversion of these forward models. In order to bypass the complexity of Bouc–Wen models, a modified MR damper model by combining the Bingham-plastic model with a refined constitutive model for MR fluids was proposed very recently (Pei et al. 2021). It is anticipated that the inverse modeling of MR damper can be facilitated by virtue of the modified MR damper model.

The remainder of this paper is structured as follows. In Sect. 2, a human-designed fuzzy logic controller (FLC-HD) is developed. In Sect. 3, an inverse modeling technique is proposed to identify the input current for MR damper to track the desired force provided by the fuzzy logic controller. Section 4 describes the main procedure of optimizing the human-designed fuzzy logic controller using the NSGA-II, and then designs a series of optimization cases by varying the definitions of membership function and rule base. In Sect. 5, the optimization results are analyzed, and the optimized fuzzy controller is combined with the proposed inverse modeling technique for constructing improved semi-active control systems, whose effectiveness and robustness are investigated by conducting a series of numerical simulations on example structures. The conclusions and prospects are summarized in Sect. 6.

## 2 Human-designed fuzzy logic controller

The FLC mainly uses linguistic instructions based on the human expert knowledge as a basis for control strategy. A fuzzy logic controller can be embedded into a closed-loop system by incorporating human expertise into linguistic *IF–THEN* rules. A classical fuzzy logic controller is mainly composed of three parts, i.e., fuzzification interface, fuzzy rule and fuzzy inference design, and defuzzification interface. A schematic view of the general architecture of a fuzzy logic controller is shown in Fig. 1.

**Fig. 1** General architecture of a classical fuzzy logic controller

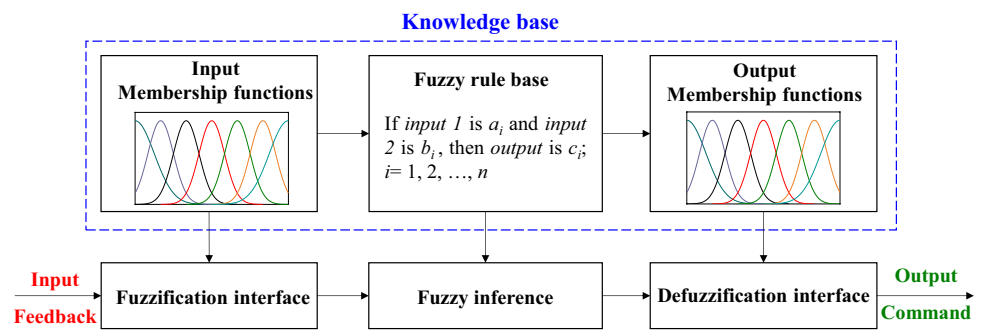


**Table 1** The linguistic variables for input and output values of the FLC

Linguistic variable	Velocity, acceleration and control force
NL	Negative large
NM	Negative medium
NS	Negative small
ZE	Zero
PS	Positive small
PM	Positive medium
PL	Positive large

**2.1 Fuzzification interface**

As shown in Fig. 1, to design a fuzzy logic controller, the first step is to choose appropriate input and output variables. In this study, the structure acceleration, which can be readily provided by accelerometers, and structural velocity are selected as fuzzy input. The control force is defined as the output variable. Next, a reasonable range of fuzzy input needs to be defined for two input variables. Here, the ranges of two input variables are respectively defined as 75% of the maximum uncontrolled velocity and acceleration responses, which are within the reasonable range (70~80%) provided in the literature (Uz and Hadi 2014; Yan and Zhou 2006). It is mainly because the structural responses under fuzzy logic control can be mostly covered by 70~80% of the uncontrolled structural responses. A too small or too large range will cause a rare or excessive use of the outermost membership functions, and thus limit the variability of the control system. Then, for convenience in defining the membership functions, the values of input variables are normalized by the corresponding ranges before entering the fuzzy logic controller. The normalized input data are then converted into linguistic variables through fuzzification. Here, the linguistic variables for both input and output values are divided into seven fuzzy variables, as listed in Table 1.

There are two types of membership functions that are often adopted for input and output variables i.e., the Gaussian and generalized bell-shaped membership functions, as

shown in Fig. 1. The main reason is that these two types of membership functions can approximate almost all other types of membership functions by appropriately defining their parameters, which are respectively defined as follows (Ahlawat and Ramaswamy 2001; Kim and Roschke 2006):

$$\mu_G = e^{\left(\frac{-(x-b)^2}{2a^2}\right)} \tag{1}$$

$$\mu_B = \frac{1}{1 + |(x - c)/d|^{2e}} \tag{2}$$

where  $a$  and  $b$  are the width (standard deviation) and central position of the Gaussian membership function, respectively;  $c$  and  $e$  are the central position and slope of the generalized bell-shaped membership function;  $d$  is the half-width of the generalized bell-shaped membership function at 0.5 membership grade.

For the human-designed fuzzy logic controller in this work, the evenly distributed Gaussian membership functions with the overlap ratio of 0.6 are adopted for describing the central parts of both input and output variables; and the spline-based Z- and S-shaped membership functions are respectively used to describe the two outermost parts of both input and output variables, as expressed by (Hanumanthakari 2021):

$$\mu_z = \begin{cases} 1, & x \leq g \\ 1 - 2\left(\frac{x-g}{h-g}\right)^2, & g \leq x \leq \frac{g+h}{2} \\ 2\left(\frac{x-h}{h-g}\right)^2, & \frac{g+h}{2} \leq x \leq h \\ 0, & x \geq h \end{cases}, \quad \mu_s = \begin{cases} 1, & x \leq p \\ 2\left(\frac{x-p}{q-p}\right)^2, & p \leq x \leq \frac{p+q}{2} \\ 1 - 2\left(\frac{x-q}{q-p}\right)^2, & \frac{p+q}{2} \leq x \leq q \\ 0, & x \geq q \end{cases} \tag{3}$$

where  $g$  and  $h$  are the central position and width of the spline-based Z-shaped membership function;  $p$  and  $q$  are the central position and width of the spline-based S-shaped membership function. For clarity, the initial membership functions for input and output variables of the human-designed fuzzy logic controller are illustrated in Fig. 2.

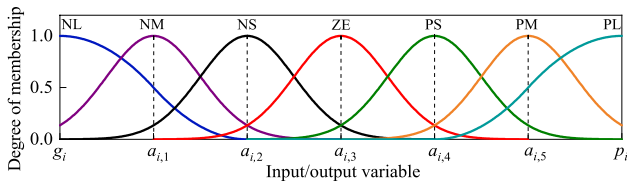


**Fig. 2** Initial membership functions for input and output variables of the human-designed fuzzy logic controller. Note:  $i = 1, 2, 3$ ;  $i = 1$  represents input 1,  $i = 2$  represents Input 2, and  $i = 3$  represents output

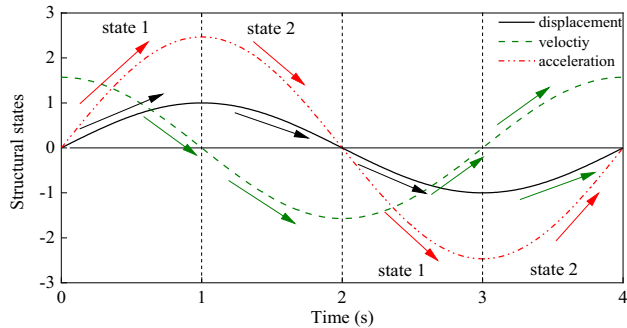


**Fig. 3** Structural motion states under a sinusoidal movement

### 2.2 Fuzzy rule and inference design

Inference engine is the kernel of a fuzzy logic controller, which characterizes the transformation from input to output. From the perspective of structural safety and comfort, in this work, the fundamental principle of devising a human-designed fuzzy logic controller is to minimize both structural displacement and acceleration. *IF-THEN* rules are employed for constructing the rule base of the fuzzy logic controller. An example of the if-premise-then-consequent statement can be expressed as:

*If* the structure velocity is *PL* and acceleration is *PL*, *then* the control force is *NL*.

To design an appropriate rule base for the fuzzy logic controller, it is necessary to observe the structural motion states and understand the system dynamics. For simplicity,

a sinusoidal movement is assumed and the corresponding structural responses, including displacement, velocity, and acceleration are illustrated in Fig. 3. As observed, one may find distinctive characteristics of structural motion states, which can be summarized as follows:

**State 1:** Structural acceleration and velocity are both positive (or negative), and the absolute value of the former is increasing while the latter is decreasing; structural displacement is increasing, indicating that the structure is moving away from the initial position. Therefore, the control force should be large to suppress the structural motion.

**State 2:** Structural acceleration and velocity are opposite in sign, and the absolute value of the former is decreasing while the latter is increasing; structural displacement is decreasing, indicating that the structure is returning toward the initial position. Therefore, the control force can be small or zero.

Based on the two states summarized above, a standard symmetric rule base is devised, as shown in Table 2.

### 2.3 Defuzzification interface

As the third part of a fuzzy logic controller, the defuzzification interface describes the mapping from the space of fuzzy outputs to crisp outputs. In this study, the center of gravity method is used to determine the crisp control output. For the  $j$ th rule of the  $i$ th input variables, the command force  $F_i$  calculated by the selected defuzzification method is expressed by (Teng et al. 2000):

$$F_i = \frac{\sum_{j=1}^{n_r} c_i^{(j)} \int \mu_i^{(j)}}{\sum_{j=1}^{n_r} \int \mu_i^{(j)}} \tag{4}$$

where  $n_r$  represents the number of fuzzy rules;  $\mu_i^{(j)}$  denotes the membership function corresponding to the output variable defined in the consequent statement of the  $j$ th rule of the  $i$ th input variable;  $c_i^{(j)}$  denotes the center of the membership function  $\mu_i^{(j)}$ .

**Table 2** Rule base for the human-designed fuzzy logic controller

	Acceleration	Velocity						
		NL	NM	NS	ZE	PS	PM	PL
NL	PL	PL	PM	PM	PS	NS	NS	
NM	PL	PL	PM	PS	ZE	NS	NM	
NS	PL	PL	PS	PS	ZE	NM	NM	
ZE	PL	PM	PS	ZE	NS	NM	NL	
PS	PM	PM	ZE	NS	NS	NL	NL	
PM	PM	PS	ZE	NS	NM	NL	NL	
PL	PM	PS	NS	NM	NM	NL	NL	

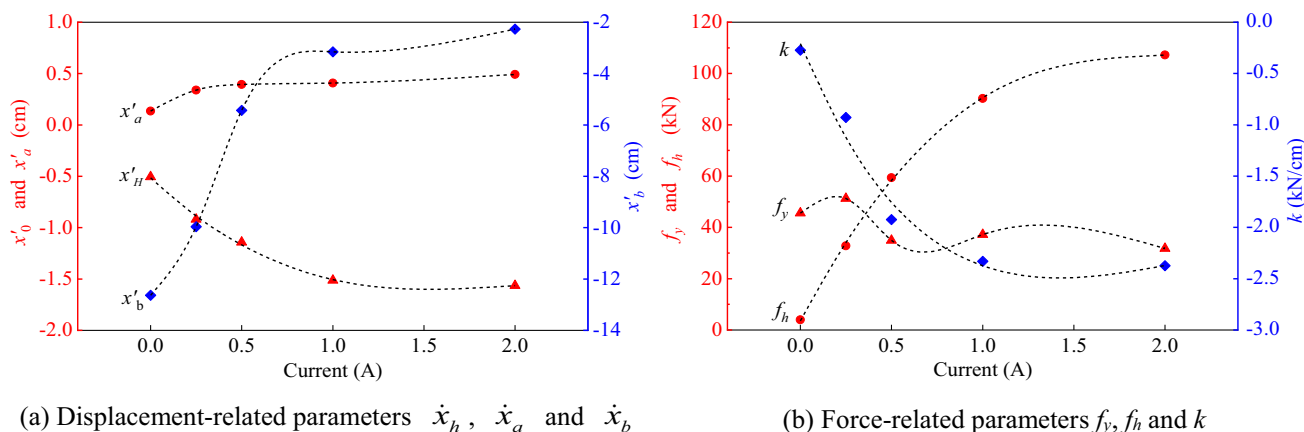


Fig. 4 Model parameters varying with input current

### 3 Inverse modeling technique for current identification of MR damper

Since the force generated by MR damper is directly controlled by the input current, an inverse model or modeling technique aimed at current identification needs to be proposed, in order to induce MR damper to produce the damping force for approaching the reference force provided by the fuzzy logic controller. In this section, an iterative force tracking technique is adopted to combine with a forward model to derive the optimum current for MR damper.

#### 3.1 Forward model

In our previous study, a simple modified Bingham-plastic model with clear physical meanings and high accuracy was proposed to characterize the dynamic behaviors of MR dampers (Pei et al. 2021). In this work, this forward model is adopted to calculate the damper force as well as further establish an inverse modeling technique for MR damper. This modified Bingham-plastic model is constructed by combing a modified Coulomb friction element in parallel with a linear spring and a hysteretic operator, which is defined as follows (Pei et al. 2021):

$$F_{mr} = kx + \lambda f_y + \xi f_h \tag{5}$$

where  $k$  is the spring stiffness;  $\lambda$  is the coefficient for controlling the low-velocity stress:

$$\lambda = \frac{2}{\pi} \text{sgn}(\dot{x}) \arctan(|\dot{x}|/\dot{x}_b) \tag{6}$$

and  $\xi$  is the hysteretic operator:

$$\xi = \arctan\left\{\frac{[\dot{x} - \dot{x}_H \text{sgn}(x)]/\dot{x}_a}{\dot{x}_a}\right\} \tag{7}$$

$f_y$  and  $f_h$  are the yielding and hysteretic forces, respectively;  $\dot{x}_a$  and  $\dot{x}_b$  are two different reference velocities for the non-dimensional purpose;  $\dot{x}_H$  is the hysteretic velocity. There are six parameters involved in this model, including three force-related parameters ( $k, f_y,$  and  $f_h$ ) and three displacement-related parameters ( $\dot{x}_H, \dot{x}_a$  and  $\dot{x}_b$ ). As shown in Fig. 4, the trends of six parameters varying with the input current have been obtained through fitting the experimental data collected from an experiment, in which a sinusoidal displacement excitation with amplitude of 2.54 cm and frequency of 0.5 Hz was applied to MR damper at various input current levels (0~2.0A) (Yang 2001). Here, the polynomial function is adopted to describe the relationships between the six parameters and input current, as expressed by:

$$k = -0.2997I^3 + 1.9563I^2 - 3.7818I - 0.236 \tag{8}$$

$$f_h = 5.101I^3 - 50.197I^2 + 131.56I + 4.0539 \tag{9}$$

$$f_y = -45.090I^3 + 152.930I^2 - 147.940I + 76.710 \tag{10}$$

$$\dot{x}_H = -0.1209I^3 + 0.8308I^2 - 1.7046I - 0.5106 \tag{11}$$

$$\dot{x}_a = -0.1347I^4 + 0.6602I^3 - 1.0982I^2 + 0.7768I + 0.204 \tag{12}$$

$$\dot{x}_b = -12.786I^4 + 61.726I^3 - 105.4I^2 + 76.802I - 23.489 \tag{13}$$

Based on the fitting parameters, the modified Bingham-plastic model is used to calculate the damper force versus time, displacement, and velocity under different input currents. The comparison of the model predictions and the fitting experimental data is shown in Fig. 5, in which a good agreement is observed, indicating the accuracy of the forward model.

### 3.2 Inverse modeling technique

An inverse model aims to provide the input current for inducing the MR damper to produce the desired control force. The most direct way to establish an inverse model is to make an inversion of a forward model. However, due to the highly nonlinear hysteretic nature, the forward MR damper models are usually composed of some complex equations, such as transcendental equation, differential equation, and power function, and they are thus difficult to be inverted for establishing an inverse model. Therefore, instead of establishing an inverse model, we choose to approach the opti-

where  $M$  and  $K$  are the mass and stiffness matrices, given by

$$M = \begin{bmatrix} 4 & 0 & 0 \\ 0 & 4 & 0 \\ 0 & 0 & 4 \end{bmatrix} \times 10^5 \text{ kg} \tag{15}$$

$$K = \begin{bmatrix} 4 & -2 & 0 \\ -2 & 4 & -2 \\ 0 & -2 & 4 \end{bmatrix} \times 10^8 \text{ N/m} \tag{16}$$

$C$  is the damping matrix and it is calculated by assuming

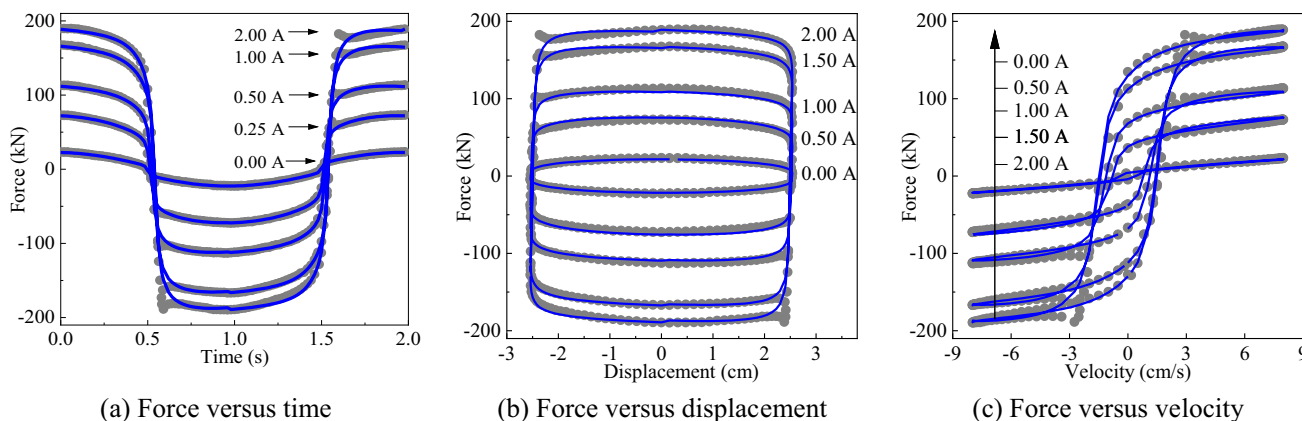


**Fig. 5** Comparison between model predictions (—) and test data (⋯) under different currents. The test data are shown as symbols reported by Yang (2001)

imum current by proposing an inverse modeling technique, which involves analyzing the motion state of the damper piston and calculating the damper force by updating the input current until the desired control force at the present instant of time is approached. For clarity, the detailed computational procedure is sketched in Fig. 6, where  $i$  denotes the present instant of time and  $j$  denotes the step of updating the input current.

### 3.3 Model validation

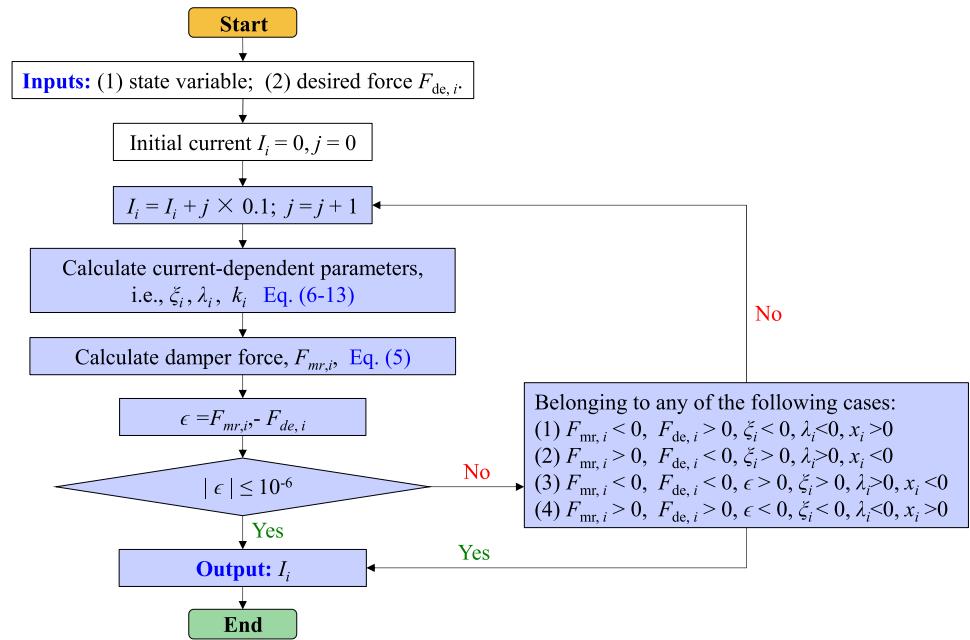
To validate the accuracy of the proposed inverse modeling technique of MR damper, in this subsection, a numerical study that involves the inverse modeling technique and the human-designed fuzzy logic controller is conducted. The example structure used here is a three-story building structure with three MR dampers installed on each floor, as shown in Fig. 7(a). With the assumption of masses lumped at floor levels, the equation of motion for this building structure subjected to seismic ground acceleration  $\ddot{x}_g$  can be written as:

$$M\ddot{X} + C\dot{X} + KX = DF_d(t) + M\ddot{x}_g \tag{14}$$

2% inherent damping and Rayleigh damping;  $X$  represents the vector of structural displacements relative to the ground, and “.” and “..” above  $X$  denote the first and second derivatives with respect to time. i.e., the vectors of velocity and acceleration.  $I$  denotes the unit vector;  $F_d$  is the force vector containing control forces provided by MR dampers;  $D$  is the matrix denoting the location of MR dampers. The NS component of the El Centro earthquake (1940) is used as the input seismic ground motion, as shown in Fig. 7(b).

The forward model presented in Sect. 3.1 is fitted based on the experimental study conducted by Yang (2001), and thus it has the maximum damper force of 200 kN under the maximum input current 2 A. Here, considering the size of the example structure, the maximum damper force is magnified into 1000 kN under the maximum input current 2 A by scaling the parameters involved in the fitted forward model. Then, numerical investigations are conducted on the proposed semi-active control scheme combining the human-designed fuzzy logic controller and the inverse modeling technique of MR damper, as illustrated in Fig. 8(a). Through a trial-and-error test, the upper bound of the output variable’s range is defined as 1400 kN, which allows the largest seismic response reduction under the

**Fig. 6** Flowchart of the inverse modeling technique of MR damper



premise that the output force is lower than 1000 kN. As a comparison, the seismic response of structure by a reference active control is calculated with the application of active tendons (actuators) commanded by the human-designed fuzzy logic controller, as illustrated in Fig. 8(b). Then, the seismic responses of the example structure obtained from two different control schemes are compared in Figs. 9(a)~(c). It is observed that the floor displacement, floor velocity, and floor acceleration responses by the proposed semi-active control scheme are in good consistency with those by the reference active control, indicating the proposed inverse modeling technique can well track the desired force. Besides, a good consistency between the control forces provided by the two control schemes shown in Fig. 9(d) has directly illustrated this point. However, some differences appear when the direction of the control force changes. The error is mainly caused by the inherent dissipative property of MR damper, which makes it

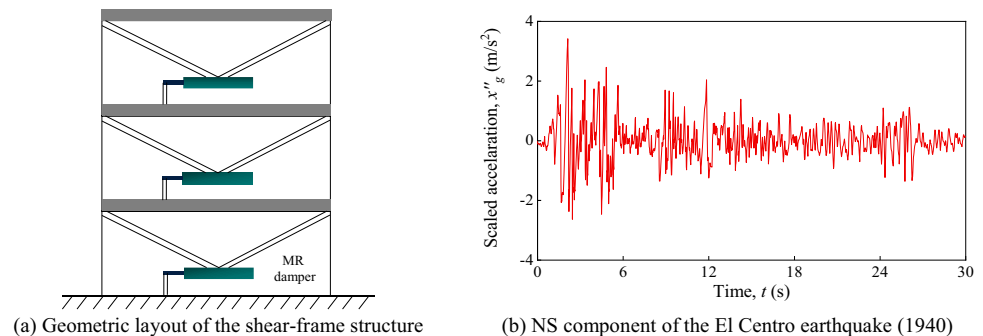
scarcely possible to output the desired optimal force all the time (Khalid et al. 2014; Xu et al. 2021).

Besides, it is worth noting that the control effectiveness of the human-designed fuzzy logic controller is limited. To achieve higher control performance, in the next section, the NSGA-II-based optimization scheme will be applied to improve the human-designed fuzzy logic controller.

#### 4 Optimization of the human-designed fuzzy logic controller using NSGA-II

To improve the performance of the human-designed fuzzy logic controller, in this section, the multiobjective GA based on the NSGA-II is adopted to optimize the membership functions and tune the fuzzy rules.

**Fig. 7** Schematic views of example structure and input seismic ground motion





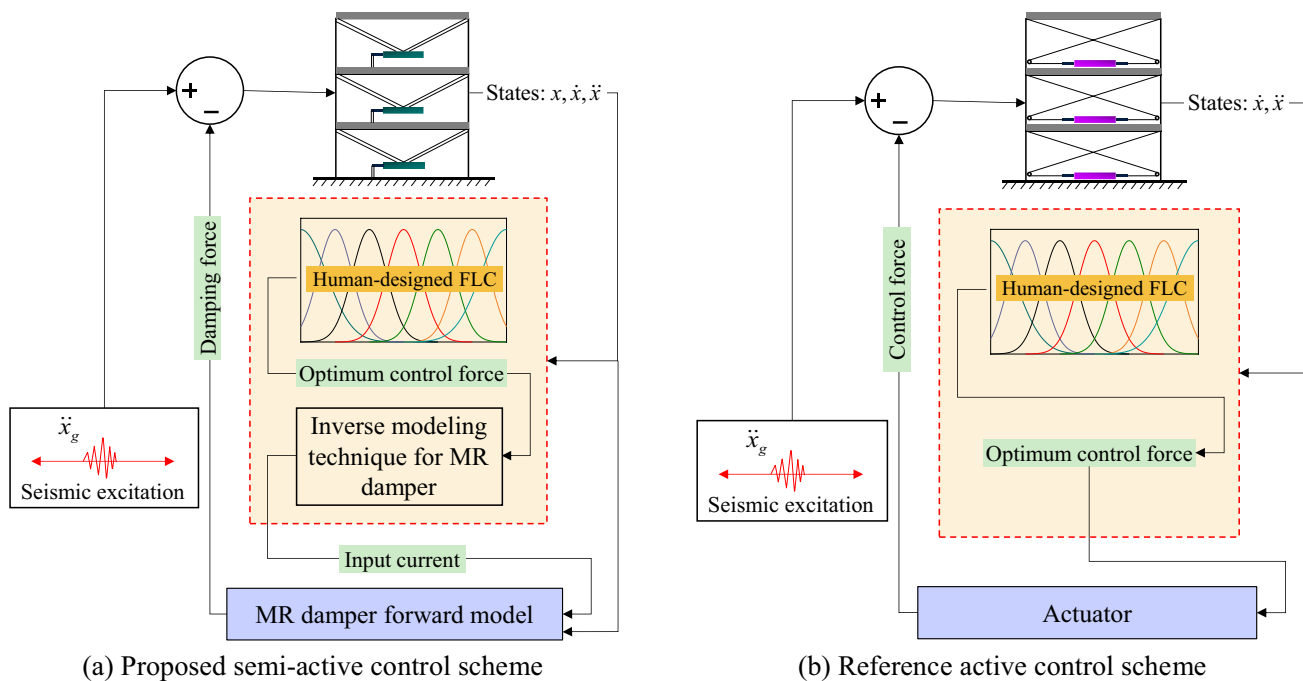


Fig. 8 Conceptual diagrams of proposed semi-active and reference active control schemes

### 4.1 Objective functions

To improve structural performance and guide the MR damper selection, five competing physical quantities are selected as control objectives in this study, including the normalized peak floor displacement and floor acceleration, the normalized root mean square (RMS) floor displacement and floor acceleration, and the normalized peak control force. The objective functions with respect to these five physical quantities are summarized in Table 3, where  $i$  denotes the floor of structure and  $t$  denotes the time;  $d_{con,i}(t)$  and  $a_{con,i}(t)$  are the  $i$ th floor displacement and floor acceleration of the controlled structure, respectively;  $d_{unc,i}(t)$  and  $a_{unc,i}(t)$  are the  $i$ th floor displacement and floor acceleration of the uncontrolled structure, respectively;  $F_{mr,i}(t)$  is the control force exerted on the  $i$ th floor at time  $t$  by the MR damper;  $F_{mr,max}$  is the maximum output of the MR damper.

### 4.2 Design variables

The performance of a fuzzy logic controller mainly relies on the choice of membership function, the definition of the rule base, and the range of output variable. Therefore, in this study, the parameters involved in membership functions, rule base, and output variable range are defined as the design variables, and the population-based approach, i.e.,

GA, is employed as the search engine. It is worth noting that there is a chance to obtain meaningless design parameters because the GA searches in a large space and uses selection, crossover, and mutation operations to ensure the diversity and optimality of solutions. To overcome this problem, some constraints need to be adopted to regulate the optimization work. As for the membership functions, it is important to maintain the initial order of the central positions of fuzzy sets. In this respect, the following inequality constraints are thus adopted for both input and output variables:

The two outermost parts of the input (output) variable are respectively described by the spline-based Z-shaped and S-shaped membership functions, then,

(1) if the Gaussian membership function is used to describe the central parts:

$$g_i = -1 \leq b_{i,1} \leq b_{i,2} \leq b_{i,3} \leq b_{i,4} \leq b_{i,5} \leq p_i = 1 \quad (i = 1, 2, 3) \tag{17}$$

(2) if the Bell-shaped membership function is used to describe the central parts:

$$g_i = -1 \leq c_{i,1} \leq c_{i,2} \leq c_{i,3} \leq c_{i,4} \leq c_{i,5} \leq p_i = 1 \quad (i = 1, 2, 3) \tag{18}$$

For the range of output variable (control force), the maximum output of MR damper  $F_{mr,max}$  of the applied semi-active control force increased by  $\pm 50\%$  is defined as the range of this optimization parameter  $F_{out}$ , as expressed by:

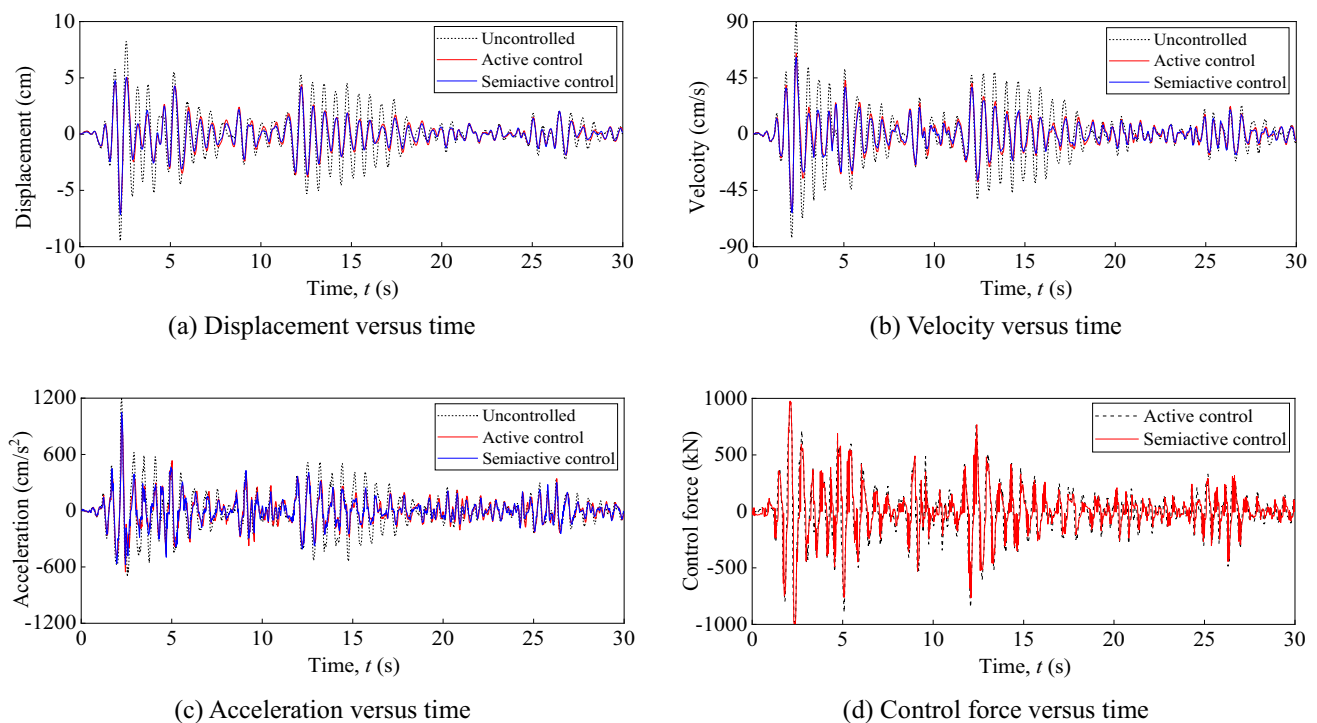


**Fig. 9** Seismic responses and control force comparisons between proposed semi-active control scheme and reference active control scheme

$$0.5F_{mr,max} \leq F_{out} \leq 1.5F_{mr,max} \quad (19)$$

### 4.3 Nondominated sorting genetic algorithm version II

Generally, the first four physical quantities (representing the mitigation of structural response) presented in Table 3 are in conflict with the last one (representing the requirement of control force), because a larger control force is often required for suppressing the structural response to a lower level. It is thus difficult to find a feasible solution that allows simultaneous minimization of all the physical quantities. In this sense, the optimization of the human-designed fuzzy logic controller can be considered as a multiobjective problem that finds optimal solutions with superior performance in terms of predefined objectives. To solve this multiobjective problem, a fast elitist nondominated sorting genetic algorithm, i.e., the NSGA-II, is adopted to optimize the human-designed fuzzy logic controller. Here, only the main optimization procedures are described. For more detailed information on the NSGA-II, please refer to reference (Deb et al. 2000).

Initially, a random parent population  $R$  of size  $N_a$  is created with consideration of the constraints defined in Eqs. (17)–(19). Each set of design variables is used to establish the corresponding fuzzy logic controller. Next, the

structural seismic responses under each fuzzy logic controller are derived to compute the objective functions and evaluate the fitness of these objective functions. Then, all the solutions are sorted based on the nondomination rank and labeled with Pareto fronts. Among the solutions with different front numbers, the one with a lower front number is better. For the solutions with the same front number, the crowding distance, which measures the distance between a solution and its neighbors in the same front, is calculated and the solution with a larger crowding distance ranks better for improving the population diversity. Subsequently, a series of fundamental GA operations including selection, crossover, and mutation are carried out to create a child population  $S$  of size  $N_b$ . Further, by combining the parent and child populations, a new population  $T$  of size  $N_a + N_b$  is obtained. This new combined population is then truncated to produce a new parent population of size  $N_a$  based on the aforementioned ranking method. The main optimization process will be repeated until the maximum number of generations is finally reached. For clarity, the optimization procedures for the FLC-based structure using NSGA-II are illustrated in Fig. 10.

### 4.4 Optimization formula

According to the statements of objective functions, design variables, and optimization algorithm, the multiobjective

**Table 3** Objective functions defined for optimization of human-designed fuzzy logic controller

Description	Objective functions
Normalized peak floor displacement	$J_1 = \frac{\max_{t,i}( d_{con,i}(t) )}{\max_{t,i}( d_{unc,i}(t) )}$
Normalized peak floor acceleration	$J_2 = \frac{\max_{t,i}( a_{con,i}(t) )}{\max_{t,i}( a_{unc,i}(t) )}$
Normalized RMS floor displacement	$J_3 = \frac{RMS_{t,i}( d_{con,i}(t) )}{RMS_{t,i}( d_{unc,i}(t) )}$
Normalized RMS floor acceleration	$J_4 = \frac{RMS_{t,i}( a_{con,i}(t) )}{RMS_{t,i}( a_{unc,i}(t) )}$
Normalized peak control force	$J_5 = \frac{\max_{t,i}( F_{mr,i}(t) )}{F_{mr,max}}$

optimization problem presented in this work can be summarized as follows:

**Find:** (1) Membership function parameters:

(a) If use Gaussian + S-shaped + Z-shaped membership functions:

Input 1 :  $a_{1,i}, b_{1,i}$  ( $i = 1, 2, 3, \dots, 5$ ),  $h_1, q_1$

Input 2 :  $a_{2,i}, b_{2,i}$  ( $i = 1, 2, 3, \dots, 5$ ),  $h_2, q_2$

Output :  $a_{3,i}, b_{3,i}$  ( $i = 1, 2, 3, \dots, 5$ ),  $h_3, q_3$

(b) If use Bell-shaped + S-shaped + Z-shaped membership functions:

Input 1 :  $c_{1,i}, d_{1,i}, e_{1,i}$  ( $i = 1, 2, 3, \dots, 5$ ),  $h_1, q_1$

Input 2 :  $c_{2,i}, d_{2,i}, e_{2,i}$  ( $i = 1, 2, 3, \dots, 5$ ),  $h_2, q_2$

Output :  $c_{3,i}, d_{3,i}, e_{3,i}$  ( $i = 1, 2, 3, \dots, 5$ ),  $h_3, q_3$

(2) Rule base:  $r_i = \{NL, NM, NS, ZE, PS, PM, PL\}$  ( $i = 1, 2, 3, \dots, n_{RB}$ )

(3) Range of output variable:  $F_{out}$

**Optimize:**  $f_1 = J_1, f_2 = J_2, f_3 = J_3, f_4 = J_4$  and  $f_5 = J_5$

**Subject to:** For Gaussian:  $g_i = -1 \leq b_{i,1} \leq b_{i,2} \leq b_{i,3} \leq b_{i,4} \leq b_{i,5} \leq p_i = 1$  ( $i = 1, 2, 3$ )

For Bell-shaped:  $g_i = -1 \leq c_{i,1} \leq c_{i,2} \leq c_{i,3} \leq c_{i,4} \leq c_{i,5} \leq p_i = 1$  ( $i = 1, 2, 3$ )

Range of output variable:  
 $0.5F_{mr,max} \leq F_{out} \leq 1.5F_{mr,max}$

To build a robust and efficient fuzzy logic controller, different optimization cases are designed by varying the type of membership functions (only Gaussian and Bell-shaped types are considered), applying the symmetric or asymmetric membership functions, and using the symmetric or asymmetric rule bases. Therefore, a total of 8 optimization cases are designed, as listed in Table 4.

## 5 Results and discussion

In this section, the NSGA-II-based multiobjective optimization method has been conducted to optimize fuzzy logic controllers for mitigating the seismic responses of both linear and nonlinear structural systems.

### 5.1 Linear structural system

The information of the linear example structure is given in Sect. 3.3. Here, the NS component of the El Centro earthquake (1940) is adopted as the external excitation; then, an optimized fuzzy controller is selected to be combined with the proposed inverse modeling technique for constructing a semi-active control scheme. The effectiveness and robustness of this optimized FLC-based semi-active control scheme are further investigated by conducting a series of numerical studies on the example structure.

#### 5.1.1 Pareto-optimal solutions

To determine an appropriate upper limit on the number of generations, the NSGA-II-based optimization is first conducted on the optimization case FLC-GSS for different numbers of generations. Based on the numerical results, the evolution process of fitness values for the normalized structural responses  $J_1, J_2, J_3$ , and  $J_4$  versus normalized control force  $J_5$  is depicted in Fig. 11. As expected, the control performance of the elite individuals is enhanced with the increasing number of generations. Besides, it is observed that, in the initial generations, the control performance exhibits a rapid improvement but shows little change in the latter generations, indicating the population gets closer and closer to the optimal front. Therefore, to ensure that an optimal front can be achieved by all the optimization cases, the maximum number of generations is specified to be 1000, and the population size is taken to contain  $N_d = 100$  individuals.

A variety of Pareto-optimal solutions are then obtained by conducting the NSGA-II-based optimization on the other

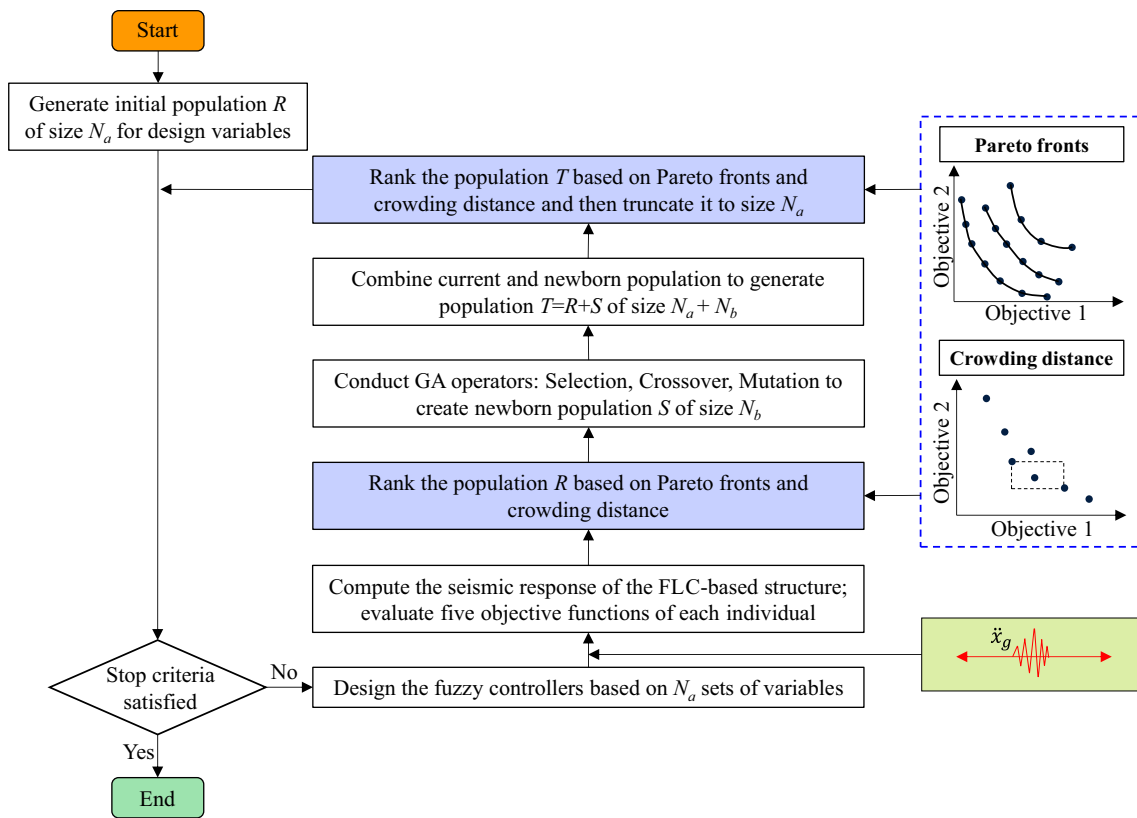


Fig. 10 Flowchart of the NSGA-II-based multiobjective optimization

Table 4 Summary of optimization cases

Cases	Variable number	Membership function				Rule base	
		Gaussian		Bell		Symmetry	Asymmetry
		Symmetry	Asymmetry	Symmetry	Asymmetry		
FLC-GSS	44	✓				✓	
FLC-GSA	68	✓					✓
FLC-GAS	62		✓			✓	
FLC-GAA	86		✓				✓
FLC-BSS	53			✓		✓	
FLC-BSA	77			✓			✓
FLC-BAS	77				✓	✓	
FLC-BAA	101				✓		✓

Note: The label of cases FLC-XYZ, in which X denotes the initial of the type of membership functions such as Gaussian, Y denotes the initial of the symmetry of membership functions such as Symmetric, and Z denotes the initial of the symmetry of rule bases such as Asymmetric

optimization cases. The Pareto fronts in terms of normalized structural responses versus normalized control force are illustrated in Fig. 12. Results show that larger control force capacity has led to more beneficial response mitigation. As a comparison, we also calculated Pareto fronts for the case using the human-designed fuzzy logic controller by

varying the range of output variable. As can be seen from Fig. 12, the optimal fronts of the optimized fuzzy controllers are generally much closer to the vertical axis than that of the human-designed fuzzy logic controller in both peak and RMS responses, indicating an improved control capacity.

In general, compared with the optimization case with symmetric membership functions (or rule base), the case with asymmetric ones possesses more variability due to the

involvement of more undetermined design variables, and thus it can provide better control performance. However, Fig. 12 shows that the optimization cases with symmetric membership functions (or rule base) can also obtain good results and some are even better than the cases with both asymmetric membership functions and rule base. A typical example can be found by comparing the FLC-GAS and FLC-GAA cases. The main reason is that the increasing number of design variables has widened the search space and thus makes it more difficult to find optimum solutions in predefined generations. Therefore, to achieve a balance between optimization efficiency and effectiveness, it is not recommended to design a fuzzy logic controller with both asymmetric membership functions and rule base.

According to Fig. 12, we can also observe that, when the normalized peak control force is larger than 0.6, the Gaussian membership function-based controllers generally show superior performance in comparison with the Bell-shaped membership function-based controllers. Conversely, when the normalized peak control force is less than 0.6, the Bell-shaped membership function-based controllers perform better. This phenomenon demonstrates that the optimized controllers with the Bell-shaped membership functions are not absolutely better than those with the Gaussian membership

functions, though there are more design variables involved in the former which can offer more variability. However, it is worth noting that the computational burden may be further increased due to the involvement of more design parameters. In this respect, the Gaussian membership function is recommended for devising a fuzzy logic controller in terms of reducing design parameters as well as providing sufficient accuracy.

### 5.1.2 Structural responses

It is noted that, in this study, the maximum output of the applied MR damper is specified as  $F_{mr,max} = 1000$  kN. Therefore, to utilize the full capacity of the MR damper, as  $J_5$  approaches 1.0, the optimized controller that shows the best performance in terms of the control objectives one concerns most should be selected. Here, we have chosen an optimized fuzzy logic controller from the Pareto-optimal solutions of the FLC-GAS case, which can achieve the minimum value in terms of the sum of  $J_1$ ,  $J_2$ ,  $J_3$ , and  $J_4$ . The selected controller is highlighted in Fig. 12. By combining the selected optimized controller with the proposed inverse modeling technique, an improved semi-active control system is constructed, and then applied to mitigate seismic responses

**Fig. 11** Normalized peak and RMS structural responses versus normalized peak control force under different numbers of generations

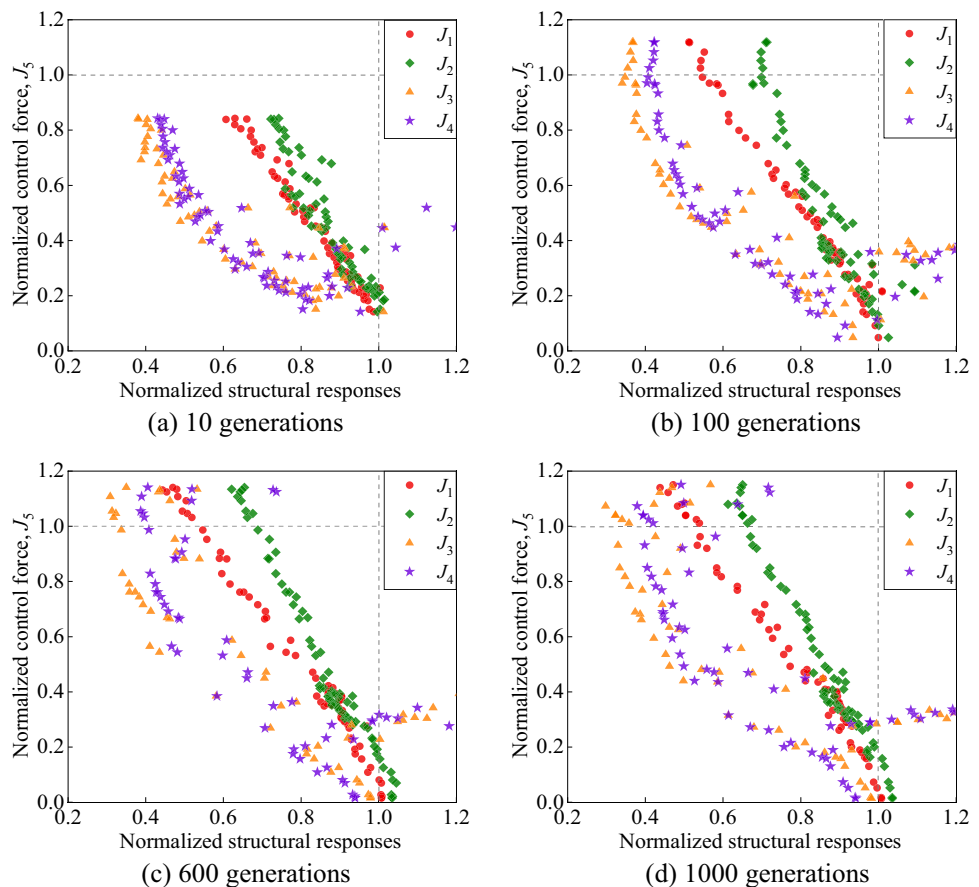
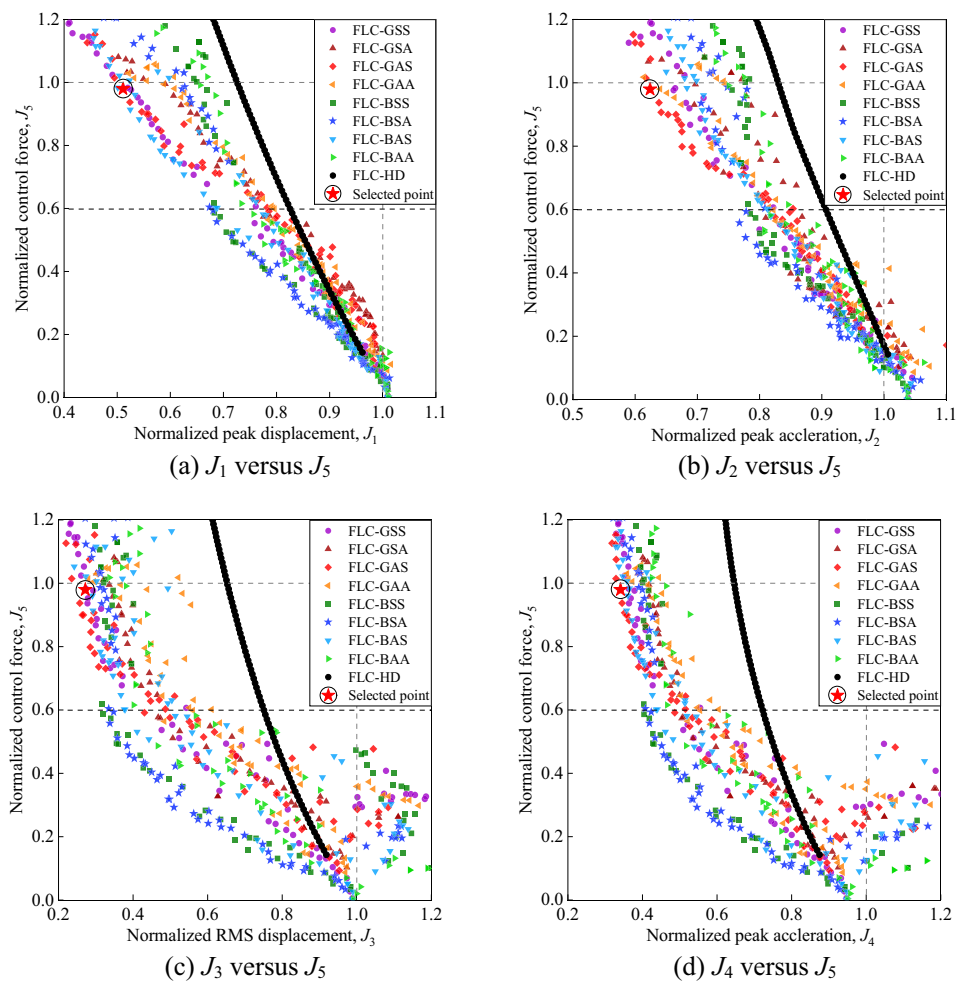


**Fig. 12** Pareto-optimal solutions for the linear structural system under different optimization cases



of the example structure. Time histories of the seismic responses of the 3rd floor and peak interstory drift along the floor of the example structure are shown in Fig. 13 for the cases of the selected FLC-GAS and the FLC, including the uncontrolled case. As qualitatively observed, the selected optimized controller can significantly reduce the structural responses, especially for the floor displacement and peak interstory drift, compared to the human-designed fuzzy logic controller.

Specifically, according to Table 6, when the selected FLC-GAS controller is applied, the four control objectives,  $J_1$ ,  $J_2$ ,  $J_3$ , and  $J_4$ , which represent the peak and RMS responses, are respectively decreased by 43.2% and 32.1%, 71.8%, and 33.5%; while for the FLC-HD case, the four indices are respectively decreased by 24.3%, 13.6%, 40.0%, and 33.7%. It can be obtained that the selected optimized controller shows superior performance in reducing peak floor displacement, peak floor acceleration, and RMS floor displacement compared to the human-designed fuzzy logic controller, except for RMS floor acceleration. Correspondingly, the control forces and input currents required by the

optimized controller are generally larger than the human-designed fuzzy logic controller, as shown in Fig. 14.

To explore the differences between the optimized FLC and human-designed FLC, the membership functions and rule base of the selected (optimized) fuzzy controller are respectively depicted in Fig. 15 and Table 5 for further analysis. By comparing with Fig. 2 and Table 2, it is found that the membership functions and rule base of the optimized fuzzy controller vary greatly from those of the human-designed fuzzy logic controller. However, if we only optimize the membership functions (or rule base) of the human-designed FLC, the obtained Pareto-optimal solutions shown in Fig. 16 indicate that optimizing membership functions can achieve better control performance compared to optimizing rule base. It is mainly because the membership functions of the human-designed FLC are assumed to be uniformly distributed without any theoretical foundation, while the rule base is formulated based on analyzing the fundamental mode of vibration.

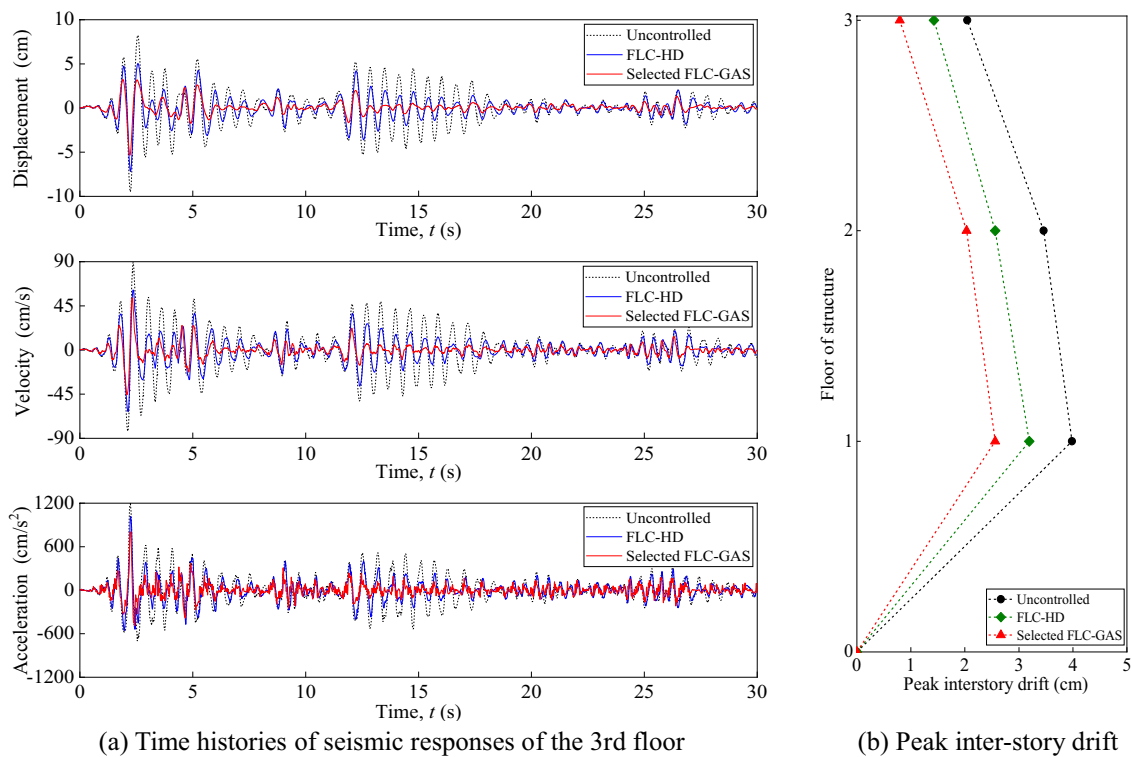


Fig. 13 Seismic responses of example structure under different control scenarios

5.1.3 Robustness of the optimized fuzzy controller

Apart from the control performance, robustness is also an important indicator for evaluating the effectiveness and performance of a control scheme, which is mainly used to measure the capability against the performance deterioration caused by uncertainties associated with structural properties and external excitations.

5.1.3.1 Influence of seismic excitations To assess the robustness of the optimized fuzzy controllers to the uncertainty associated with external excitations, the MR damper-based example structure subjected to two other earthquakes, i.e., Kobe (1995) and Northridge (1994), are investigated.

The two recorded seismic accelerograms are scaled to have the same peak ground acceleration as that of the El Centro (1940) earthquake which is used for optimization. Qualitative and quantitative comparisons with respect to the structural responses obtained from different control scenarios are shown in Fig. 17 and Table 6, respectively. It is observed that both the FLC-HD and the selected FLC-GAS controllers are robust to the uncertainties of seismic excitations; and, the selected FLC-GAS controller still shows superior performance in mitigating seismic responses compared to the human-designed fuzzy logic controller when the seismic excitation is varied.

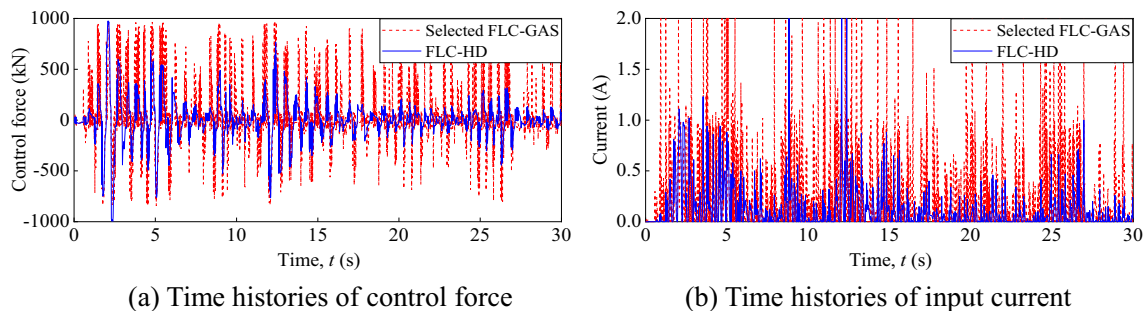


Fig. 14 Time histories of control force and input current of MR damper on the 3rd floor under different control scenarios

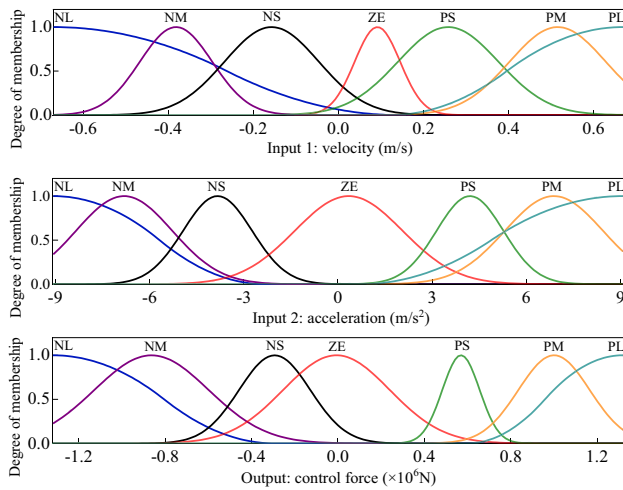


Fig. 15 Membership function obtained from selected FLC-GAS

**5.1.3.2 Influence of structural properties** To assess the robustness of the optimized fuzzy controllers to the uncertainty associated with structural properties, structural responses of MR damper-based example structure using the selected FLC-GAS and FLC-HD controllers are, respectively, computed for stiffness degradations of 15%,

25%, and 35%. The corresponding structural responses in terms of peak interstory drift are depicted in Fig. 18. As can be seen, both the selected fuzzy controller and the human-designed fuzzy logic controller can effectively reduce the seismic-induced structural responses when the example structure experiences 15%, 25%, and 35% stiffness degradations, indicating their robustness to the uncertainties of structural properties. Besides, it is observed that the selected fuzzy controller can reduce the structural responses to a relatively larger extent compared with the human-designed fuzzy logic controller.

## 5.2 Nonlinear structural system

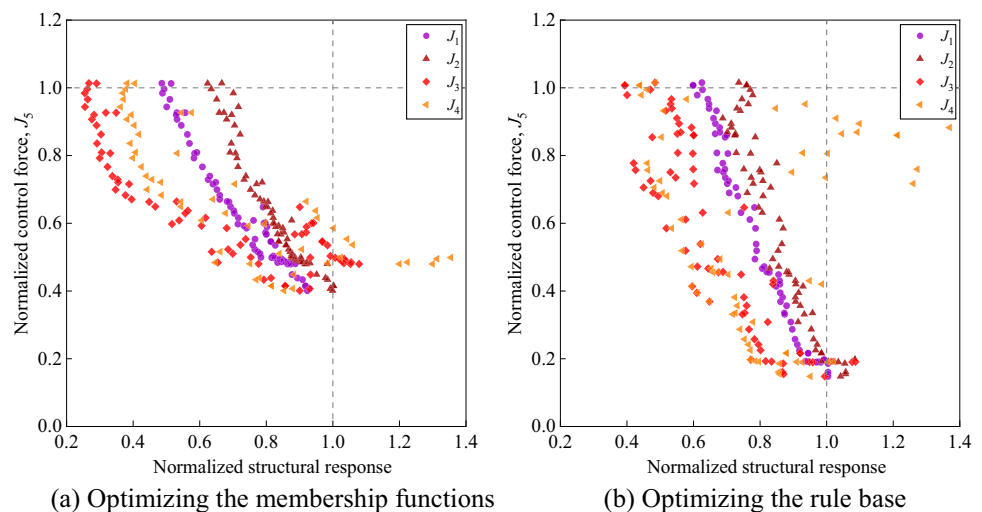
### 5.2.1 Structure model

The example structure explored here is a ten-story nonlinear shear frame equipped with MR dampers, as shown in Fig. 19(a). The lumped masses of the structure are given as  $m_1 = 5.18$ ,  $m_2 = 4.92$ ,  $m_3 = 4.59$ ,  $m_4 = 4.13$ ,  $m_5 = 4.00$ ,  $m_6 = 4.00$ ,  $m_7 = 4.00$ ,  $m_8 = 4.00$ ,  $m_9 = 4.00$ ,  $m_{10} = 4.00$  ( $\times 10^8$  kg), and the initial interstory stiffnesses are given as  $k_1 = 2.92$ ,  $k_2 = 2.11$ ,  $k_3 = 1.96$ ,  $k_4 = 1.82$ ,  $k_5 = 1.55$ ,  $k_6 = 1.55$ ,  $k_7 = 1.55$ ,  $k_8 = 1.55$ ,  $k_9 = 1.55$ ,  $k_{10} = 1.55$

Table 5 Rule base of selected FLC-GAS

	Acceleration		Velocity					
	NL	NM	NS	ZE	PS	PM	PL	
NL	PM	NS	NS	PM	ZE	PS	ZE	
NM	PM	ZE	NS	PS	PS	PM	NM	
NS	PM	NS	PM	PS	NM	ZE	ZE	
ZE	PM	PM	PM	NL	NM	NM	NM	
PS	ZE	ZE	PM	NS	NM	PS	NM	
PM	PM	NM	NS	NS	PS	ZE	NM	
PL	ZE	NS	ZE	NM	PS	PS	NM	

Fig. 16 Pareto fronts obtained by only optimizing the membership functions or rule base





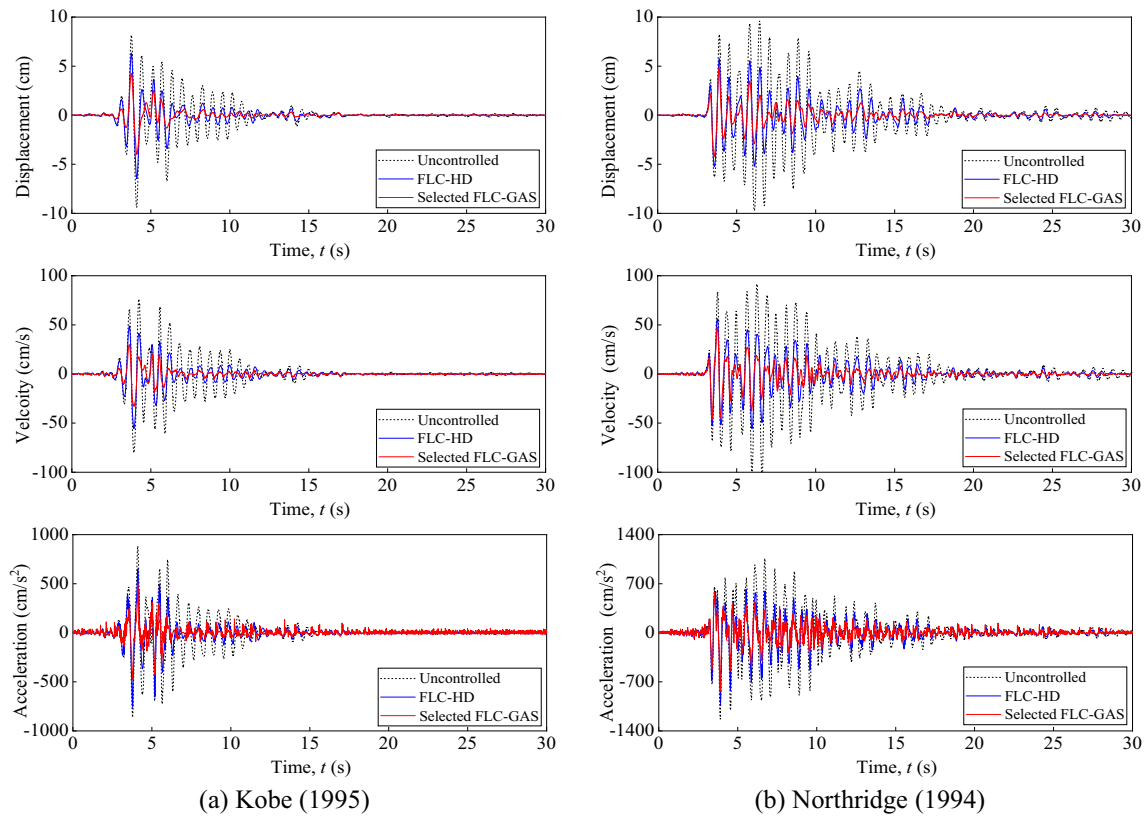


Fig. 17 Time histories of seismic responses of the 3rd floor under different control scenarios and earthquakes

Table 6 Comparison of control objectives under different control scenarios and earthquakes

Control objective	El Centro (1940)		Kobe (1995)		Northridge (1994)	
	FLC-HD	Selected FLC-GAS	FLC-HD	Selected FLC-GAS	FLC-HD	Selected FLC-GAS
$J_1$	0.757	0.568	0.687	0.456	0.594	0.496
$J_2$	0.864	0.679	0.858	0.531	0.826	0.676
$J_3$	0.600	0.288	0.501	0.272	0.474	0.240
$J_4$	0.663	0.665	0.546	0.459	0.542	0.421

( $\times 10^5$  N/m). Rayleigh damping is utilized here, with the damping ratio being 0.05. The nonlinear interstory hysteretic behavior is represented by the Bouc–Wen model (Ma et al. 2004), as shown in Fig. 19(b). The parameters of the Bouc–Wen model can refer to (Peng et al. 2021b; Li et al. 2011). The maximum damping capacity of the MR damper is also set as 1000 kN. The NS component of the El Centro earthquake (1940) is used as the input seismic ground motion.

For high-rise buildings, more MR dampers are often required and the layout of MR dampers needs to be well designed. In this respect, apart from the FLC parameters, the damper deployment, i.e., the quantity of MR dampers installed on each floor, is also considered for optimization

here, in an attempt to achieve a better control performance. Therefore, more design parameters need to be optimized, which has increased the dimension of the optimization problem. In the meantime, it is worth noting that, compared with the linear structural system, the optimization for the nonlinear structural system is more computationally demanding due to the nonlinearity and associated complexity involved in structural dynamics.

According to the analysis results obtained from the linear structure, the Gaussian membership function is recommended for constructing and optimizing fuzzy logic controllers in terms of accuracy and fewer undetermined parameters; and there is no need to simultaneously consider the asymmetry in both membership functions and

**Fig. 18** Peak interstory drift under different stiffness degradation levels

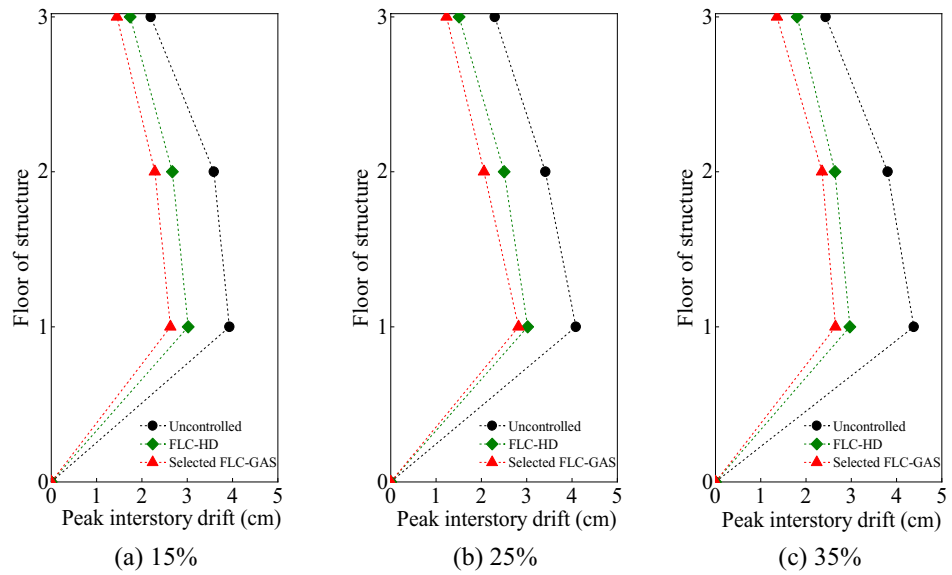
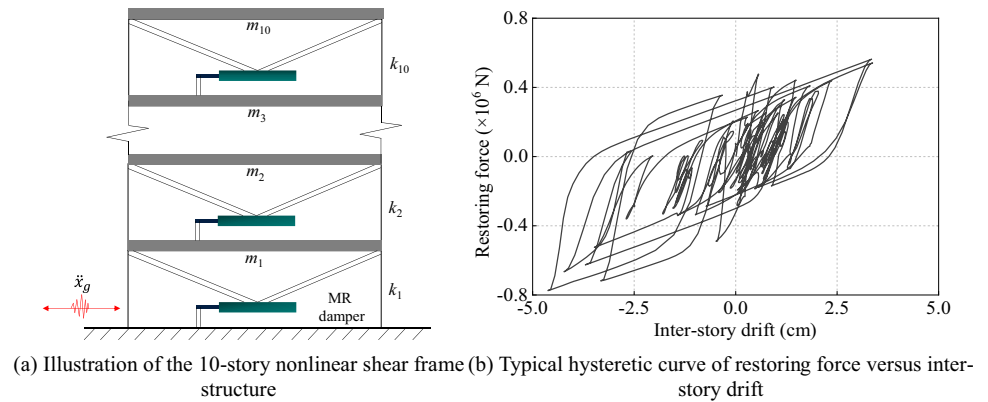


**Fig. 19** Basic information of the ten-story nonlinear shear frame structure



rule base. Hence, from the perspective of optimization efficiency and effectiveness, only three optimization cases are considered for the nonlinear structural system, as listed in Table 7. It is worth noting that, in the first optimization case, the human-designed fuzzy rules are used and only the parameters involved in membership functions and damper deployment are considered, because the human-designed fuzzy rules have been proved to be more effective than the human-designed membership functions in FLC design. Besides, in view of structural size restriction and economical aspect, two constraints are considered for restricting the quantities of MR dampers on each floor and total floors, i.e.,

$$\text{Subject to: } \begin{cases} 0 \leq p_i \leq 3 & (i = 1, \dots, 10) \\ N_{\text{mr}} = \text{sum}(p_i) \leq 10 & (i = 1, \dots, 10) \end{cases} \quad (20)$$

where  $p_i$  denotes the number of MR dampers on the  $i$ th floor and  $N_{\text{mr}}$  represents the total number of MR dampers.

### 5.2.2 Pareto-optimal solutions

The final Pareto-optimal solutions in the form of normalized structural responses versus normalized control force for the nonlinear structural system obtained from different optimization cases are illustrated in Fig. 20. It is observed that the Pareto fronts of the nonlinear structural system show more irregularity and complexity compared with those of the linear structural system, which is mainly attributed to the nonlinearity involved in the structural dynamics of the former. Besides, it is noticed that the control force ranges provided by the FLC-GAS-D and the FLC-GSA-D optimization cases are relatively smaller than that of the FLC-GA-D optimization case. Then, below the threshold line of maximum damper force 1000 kN ( $J_5 = 1.0$ ), the Pareto-optimal solutions obtained from the FLC-GA-D optimization case are relatively closer to the vertical axis than those obtained from the other two cases, indicating a better performance in structural control. This phenomenon has proved again that the proposed fuzzy rules are effective in constructing optimal

**Table 7** Summary of optimization cases for the nonlinear structural system

Cases	Variable number	Design variables		
		Membership function	Rule base	MR damper deployment
FLC-GA-D	47	Asymmetric Gaussian	Human-designed rules	Considered
FLC-GAS-D	72	Asymmetric Gaussian	Symmetric rules	Considered
FLC-GSA-D	78	Symmetric Gaussian	Asymmetric rules	Considered

fuzzy logic controllers for structural control. With the proposed fuzzy rules, one only needs to optimize the parameters involved in membership functions for FLC design, which can largely reduce the number of design parameters.

The objective functions versus the total number of MR dampers obtained from different optimization cases are

compared in Fig. 21. As can be seen, for all three optimization cases, the structural responses ( $J_1 \sim J_4$ ) show a decreasing trend with the increasing number of MR dampers, especially for the displacement responses (see  $J_1$  and  $J_3$  in the three subfigures); and when the total number of MR dampers remains unchanged, e.g., the total number of MR dampers

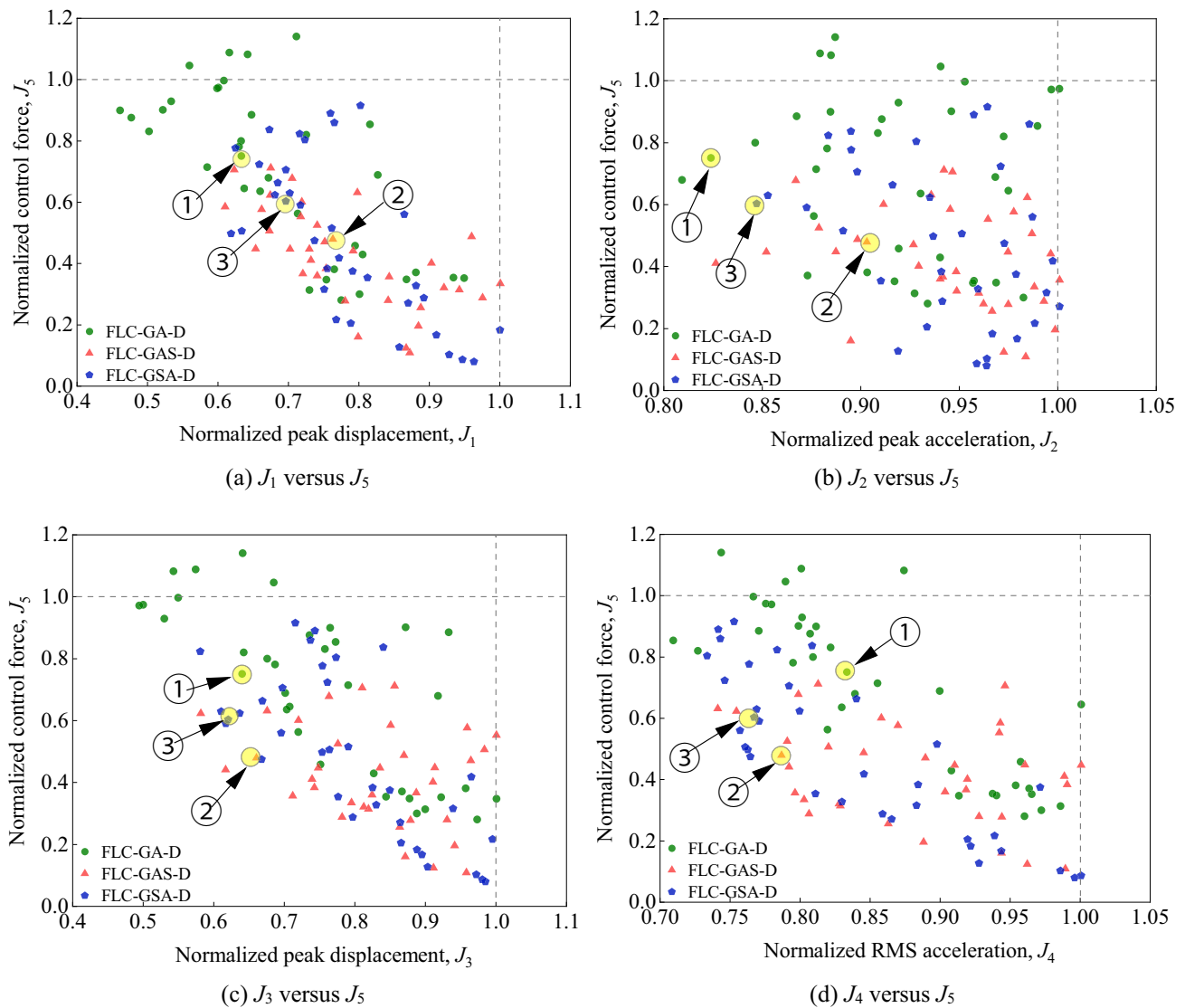


**Fig. 20** Pareto-optimal solutions for the nonlinear structural system under different optimization cases

taking 10, the structural responses vary owing to the variations in damper distribution (different deployments of MR dampers on floors) and FLC configuration (different design variables as shown in Table 7).

To further investigate the damper layout properties, the optimal solutions to the damper deployment are first normalized by the bounds of the design space and then mapped into a 10-dimensional polygon loop ( $p_1$  to  $p_{10}$  denotes the 1st floor to the 10th floor), as shown in Fig. 22. In this polygon loop-based design space, the upper and lower bounds of a design variable are respectively represented by the outer and inner rings of the polygon loop (the point on the inner ring denotes none of dampers; the point on the outer ring denotes 3 dampers). It is observed that MR dampers are mainly installed on the bottom floors especially in the optimization cases of FLC-GAS-D and FLC-GSA-D, as large seismic force is concentrated on the bottom floors.

Subsequently, to probe the characteristics of the optimized fuzzy logic controllers, the optimal solutions to the membership functions and fuzzy rules obtained from the 3 optimization cases are collected here for analysis. For clarity, the solutions to the membership functions are first normalized by the bounds of the design space and then mapped into a 37-dimensional polygon (representing 37 design parameters involved in membership functions). In the polygon-based design space, the upper and lower bounds of a design variable are respectively represented by the vertex and the center of the polygon; see Fig. 23. Subsequently, similar operations have been conducted to the solutions of the fuzzy rules; see Fig. 24, in which 7 solid and dash circles from the outer loop to the inner

loop respectively represent PL, PM, PS, ZE, NS, NM, and NL, respectively. As a comparison, the proposed fuzzy rules are also illustrated in Fig. 24, which are represented by red hollow triangles connected by red dash lines. It is observed that the solutions to the membership functions obtained from the FLC-GAS-D optimization case mainly concentrate in the central area of the design space, while those obtained from the other two cases show more dispersion, especially for the FLC-GA-D case; see Fig. 23a. Besides, the solutions to the fuzzy rules from the FLC-GAS-D optimization case also show more concentration than those obtained from the FLC-GSA-D optimization case. Therefore, the solution space of the FLC-GAS-D optimization case is relatively more narrowed compared with the other two optimization cases. This has explained the reason why the Pareto-optimal solutions derived from the FLC-GAS-D optimization case are not as good as those from the other two cases.

### 5.2.3 Robustness of the optimized fuzzy controller

As the multiobjective optimization approach provides a set of Pareto-optimal solutions, an engineer is able to select an appropriate design for the specific performance requirement. Here, the solution, which can achieve the minimum value in terms of the sum of  $J_1$ ,  $J_2$ ,  $J_3$ , and  $J_4$ , is selected from each optimization case. Therefore, three solutions have been respectively selected from the FLC-GA-D, FLC-GAS-D and FLC-GSA-D optimization cases, denoted as ①, ②, and ③; see Fig. 20. The damper deployment, rule base and membership

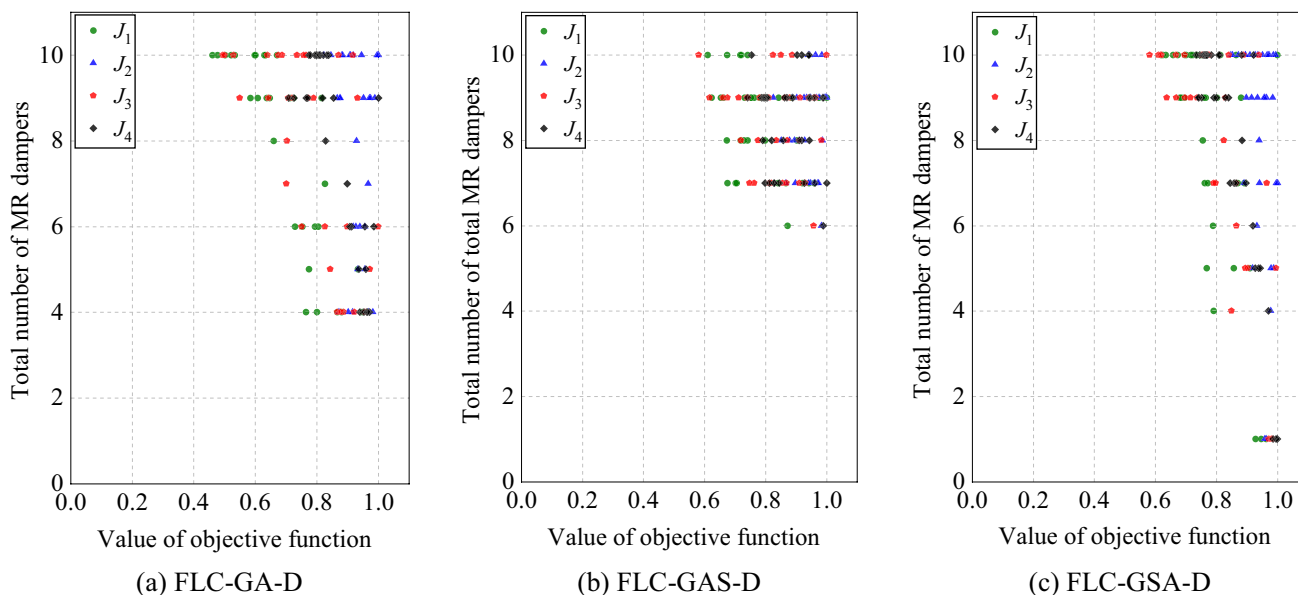


Fig. 21 Objective functions versus the total number of MR dampers for different optimization cases

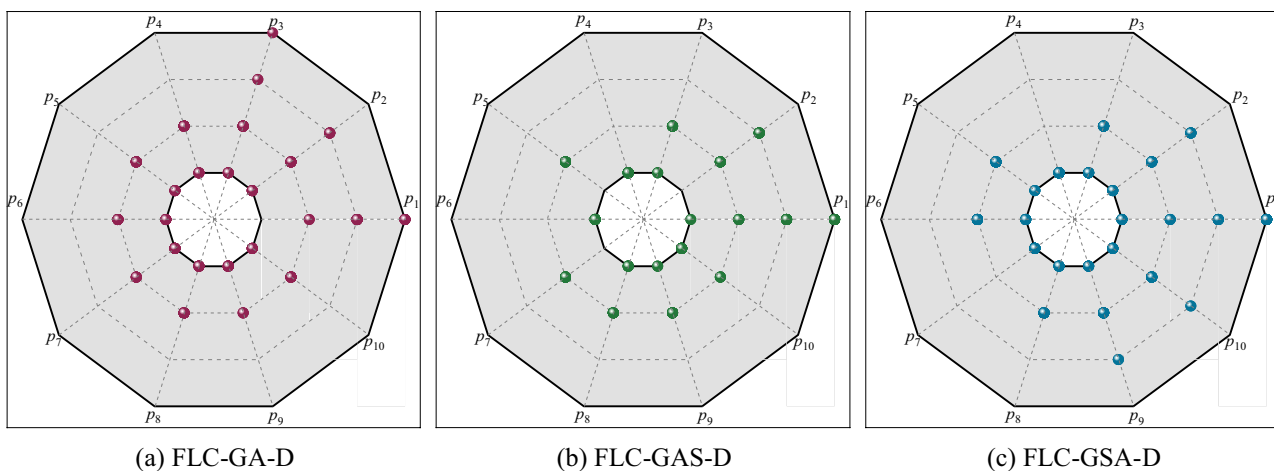


Fig. 22 Optimal solutions to the damper deployment

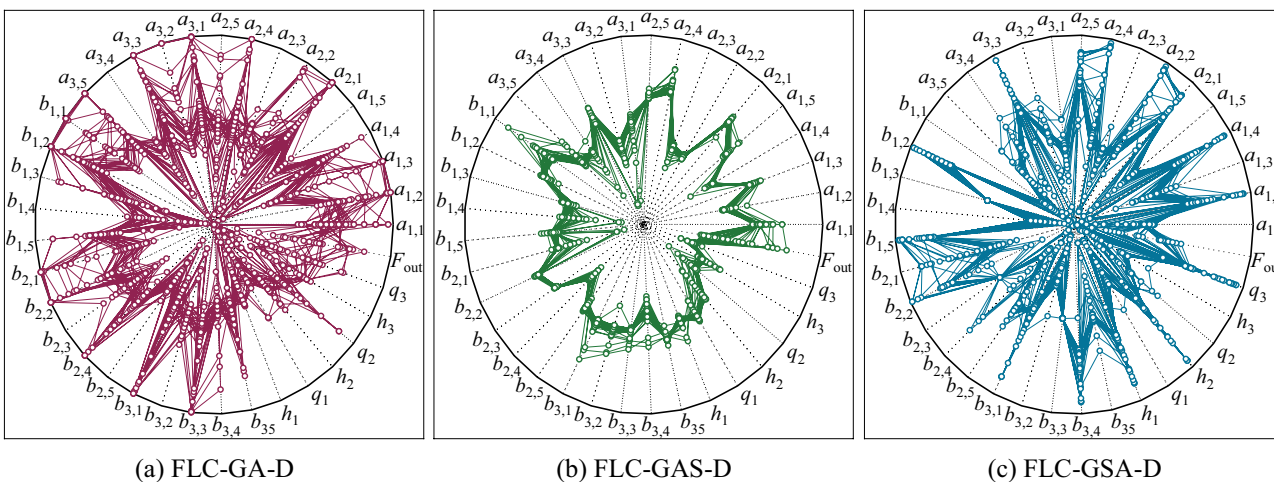


Fig. 23 Optimal solutions to the membership functions

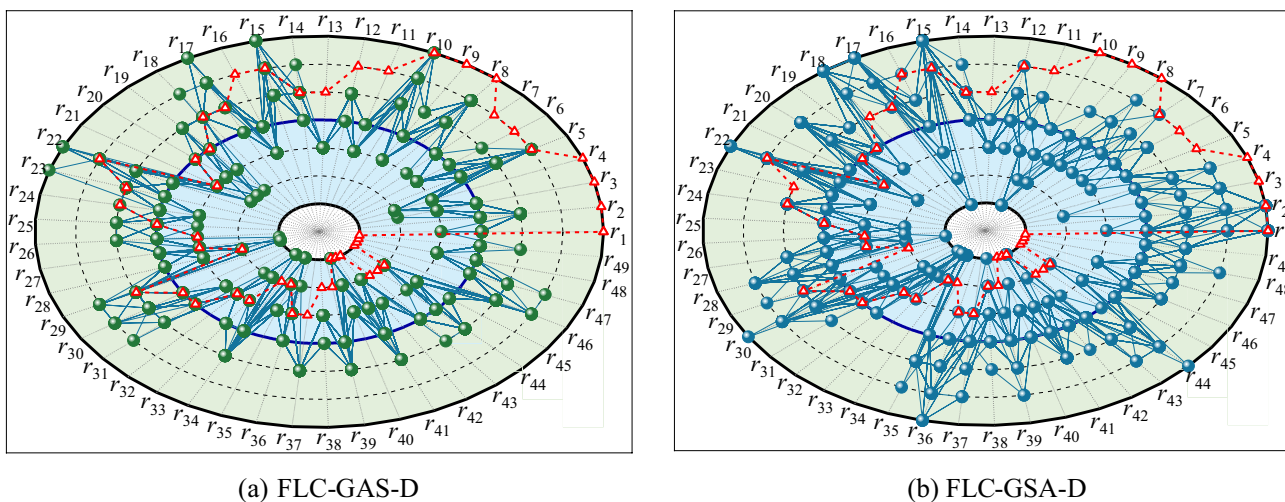


Fig. 24 Optimal solutions to the rule base

function configuration corresponding to the three selected solutions are respectively illustrated in Fig. 25a–c.

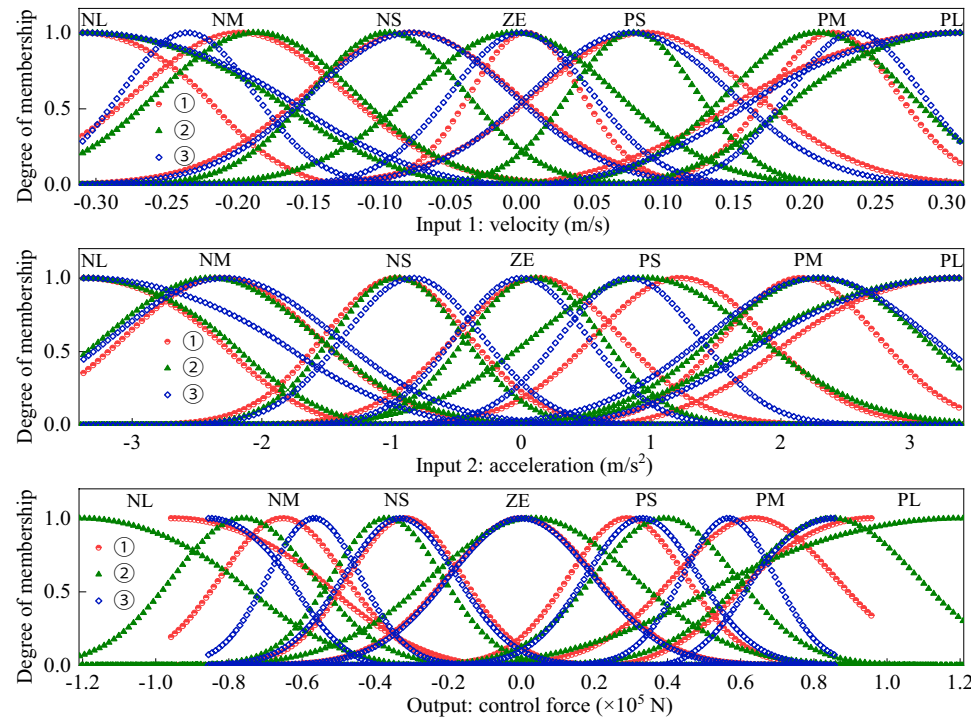
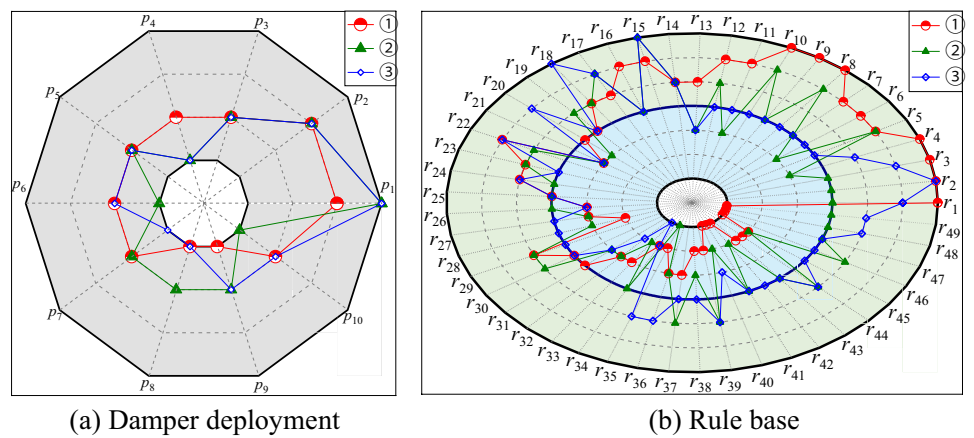
Three fuzzy logic controllers are then constructed according to the selected solutions. By combining the constructed controllers with the proposed inverse modeling technique, 3 improved semi-active control systems are obtained for mitigating the seismic responses of the non-linear structure. The controllers' robustness to the uncertainties involved in structural stiffness and earthquake excitations are then explored. The structural responses of the original controlled structure have been compared with those of the same controlled structure with 15%, 25%, and 35% stiffness degradations or the same controlled structure under different earthquake ground motions, as shown in Figs. 26 and 27, in which a good agreement can be

observed, indicating the robustness of the developed semi-active control systems to the uncertainties in structural properties and external loadings.

### 6 Conclusions

An improved semi-active control scheme is developed in this study by combing the NSGA-II optimized FLC with a newly proposed inverse modeling technique of MR damper. For validation and comparison, two example structures equipped with MR dampers are addressed. The main conclusions are summarized as follows:

**Fig. 25** Damper deployment, rule base and membership function configuration of the three selected solutions



(c) Membership function configuration

- (1) A human-designed fuzzy logic controller is developed by assuming uniformly distributed membership functions and applying the law of the fundamental vibration mode-based fuzzy rules. The proposed rule base has been proved to be useful in the FLC design.
- (2) Based on the modified Bingham-plastic model, an inverse modeling technique is developed for identifying the input current of MR damper.
- (3) Various sets of Pareto-optimal solutions have been obtained from different optimization cases. Comparison results show that optimized fuzzy controllers show much better control performance than the human-designed one.
- (4) To achieve a balance between optimization efficiency and effectiveness, it is not recommended to design a fuzzy logic controller with both asymmetric membership functions and rule base.
- (5) Compared with the Bell-shaped membership function, the Gaussian membership function is recommended for the FLC design in terms of optimization efficiency and effectiveness.
- (6) The improved semi-active control system shows desired capability and robustness in mitigating seismic responses of both the linear and nonlinear structural systems.

An effective and robust semi-active control scheme has been proposed in this study, but the corresponding numerical investigations are limited to linear and nonlinear plane structures. An in-depth analysis of the proposed control scheme in real-life engineering structures is an ongoing work.

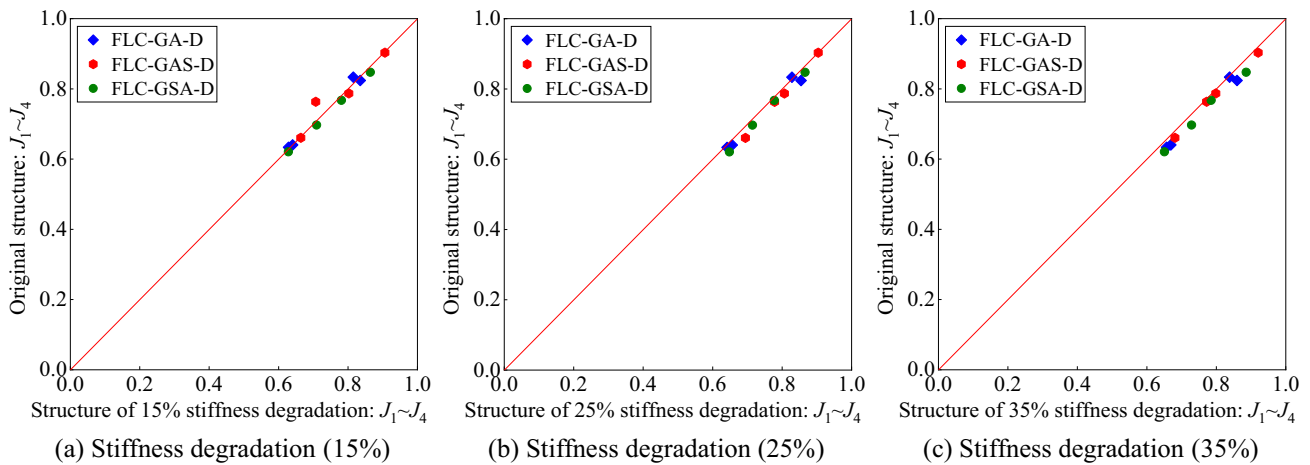
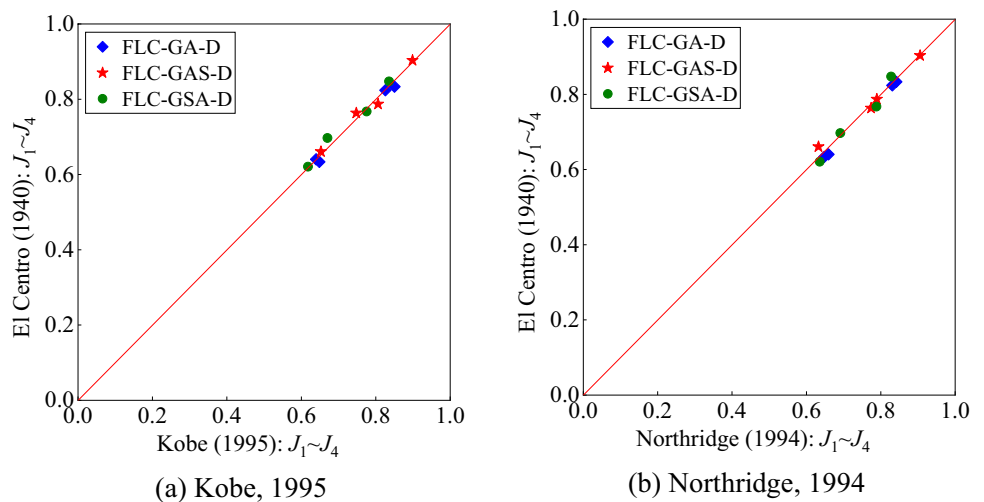


**Fig. 26** Comparison between structural responses of the original controlled structure and the same controlled structure under different stiffness degradation levels

**Fig. 27** Comparison between structural responses of the same controlled structure under different earthquake ground motions



**Acknowledgements** The supports of the National Natural Science Foundation of China (Grant No. 51878505) and Natural Science Foundation of Shanghai (Grant No. 21ZR1425500) are highly appreciated.

## Declarations

**Conflict of interest** On behalf of all authors, the corresponding author states that there is no conflict of interest.

**Replication of results** The details of the proposed methodology and of the specific values of the parameters considered have been provided in the paper. Hence, we are confident that the results can be reproduced. Readers interested in the source code are encouraged to contact the authors by e-mail.

## References

- Ahlatw AS, Ramaswamy A (2001) Multiobjective optimal structural vibration control using fuzzy logic control system. *J Struct Eng* 127:1330–1337. [https://doi.org/10.1061/\(ASCE\)0733-9445\(2001\)127:11\(1330\)](https://doi.org/10.1061/(ASCE)0733-9445(2001)127:11(1330))
- Ali SF, Ramaswamy A (2008) GA-optimized FLC-driven semi-active control for phase-II smart nonlinear base-isolated benchmark building. *Struct Control Health Monit* 15:797–820. <https://doi.org/10.1002/stc.272>
- Ali SF, Ramaswamy A (2009) Optimal fuzzy logic control for MDOF structural systems using evolutionary algorithms. *Eng Appl Artif Intell* 22:407–419. <https://doi.org/10.1016/j.engappai.2008.09.004>
- Azizi M, Ejlali RG, Mousavi Ghasemi SA, Talatahari S (2019) Upgraded Whale Optimization Algorithm for fuzzy logic based vibration control of nonlinear steel structure. *Eng Struct* 192:53–70. <https://doi.org/10.1016/j.engstruct.2019.05.007>
- Bathaei A, Zahrai SM, Ramezani M (2018) Semi-active seismic control of an 11-DOF building model with TMD+ MR damper using type-1 and-2 fuzzy algorithms. *J Vib Control* 24:2938–2953
- Behboodi S, Bitaraf M, Nafisifard M (2021) Prevention of low-cycle fatigue damage using adaptive control approach and magnetorheological dampers. *Structures* 33:554–566. <https://doi.org/10.1016/j.istruc.2021.04.085>
- Cha Y-J, Zhang J, Agrawal AK, Dong B, Friedman A, Dyke SJ, Ricles J (2013) Comparative studies of semiactive control strategies for MR dampers: pure simulation and real-time hybrid tests. *J Struct Eng* 139:1237–1248
- Chakraborty S, Debbarma R (2011) Stochastic earthquake response control of structures by liquid column vibration absorber with uncertain bounded system parameters. *Struct Saf* 33:136–144
- Choi KM, Cho SW, Jung HJ, Lee IW (2004) Semi-active fuzzy control for seismic response reduction using magnetorheological dampers. *Earthq Eng Struct Dyn* 33:723–736. <https://doi.org/10.1002/eqe.372>
- Deb K, Agrawal S, Pratap A, Meyarivan T (2000) A fast elitist non-dominated sorting genetic algorithm for multi-objective optimization: NSGA-II. In: International conference on parallel problem solving from nature. Springer, pp 849–858
- Dounis AI, Tiropanis P, Syrcos GP, Tseles D (2007) Evolutionary fuzzy logic control of base-isolated structures in response to earthquake activity. *Struct Control Health Monit* 14:62–82. <https://doi.org/10.1002/stc.83>
- Dyke SJ, Spencer BF Jr, Sain MK, Carlson JD (1996) Modeling and control of magnetorheological dampers for seismic response reduction. *Smart Mater Struct* 5:565–575. <https://doi.org/10.1088/0964-1726/5/5/006>
- Dyke SJ, Spencer BF Jr, Sain MK, Carlson JD (1998) An experimental study of MR dampers for seismic protection. *Smart Mater Struct* 7:693–703. <https://doi.org/10.1088/0964-1726/7/5/012>
- Dyke S, Spencer B (1997) A comparison of semi-active control strategies for the MR damper. In: Proceedings Intelligent Information Systems IIS'97. IEEE, pp 580–584
- Ghadimi B, Taghikhany T (2021) Dynamic response assessment of an offshore jacket platform with semi-active fuzzy-based controller: a case study. *Ocean Eng*. <https://doi.org/10.1016/j.oceaneng.2021.109747>
- Hanumanthakari S (2021) Comparative analysis of different types of membership functions for fuzzy logic controller in direct torque control of induction motor. In: Intelligent Computing in Control and Communication. Springer, pp 405–416
- Housner G, Bergman LA, Caughey TK, Chassiakos AG, Claus RO, Masri SF, Skelton RE, Soong TT, Spencer BF, Yao JT (1997) Structural control: past, present, and future. *J Eng Mech* 123:897–971
- Huang Z-S, Wu C, Hsu D-S (2009) Semi-active fuzzy control of mr damper on structures by genetic algorithm. *J Mech* 25:N1–N6
- Jansen LM, Dyke SJ (2000) Semiactive control strategies for MR dampers: comparative study. *J Eng Mech* 126:795–803
- Jung HJ, Choi KM, Spencer BF Jr, Lee IW (2006) Application of some semi-active control algorithms to a smart base-isolated building employing MR dampers. *Struct Control Health Monit* 13:693–704. <https://doi.org/10.1002/stc.106>
- Khalid M, Yusof R, Joshani M, Selamat H, Joshani M (2014) Nonlinear identification of a magneto-rheological damper based on dynamic neural networks. *Comput-Aided Civ Infrastruct Eng* 29:221–233
- Kim HS, Roschke PN (2006) Fuzzy control of base-isolation system using multi-objective genetic algorithm. *Comput-Aided Civ Infrastruct Eng* 21:436–449. <https://doi.org/10.1111/j.1467-8667.2006.00448.x>
- Kim HS, Roschke PN (2007) GA-fuzzy control of smart base isolated benchmark building using supervisory control technique. *Adv Eng Softw* 38:453–465. <https://doi.org/10.1016/j.advengsoft.2006.10.004>
- Li J, Peng Y, Chen J (2010) A physical approach to structural stochastic optimal controls. *Probab Eng Mech* 25:127–141
- Li J, Peng Y, Chen J (2011) Nonlinear stochastic optimal control strategy of hysteretic structures. *Struct Eng Mech* 38:39–63. <https://doi.org/10.12989/sem.2011.38.1.039>
- Ma F, Zhang H, Bockstedte A, Foliente GC, Paevere P (2004) Parameter analysis of the differential model of hysteresis. *J Appl Mech Trans ASME* 71:342–349. <https://doi.org/10.1115/1.1668082>
- Marinaki M, Marinakis Y, Stavroulakis GE (2011) Fuzzy control optimized by a multi-objective particle swarm optimization algorithm for vibration suppression of smart structures. *Struct Multidisc Optim* 43:29–42. <https://doi.org/10.1007/s00158-010-0552-4>
- Mehrkian B, Bahar A, Chaibakhsh A (2019) Semiactive conceptual fuzzy control of magnetorheological dampers in an irregular base-isolated benchmark building optimized by multi-objective genetic algorithm. *Struct Control Health Monit*. <https://doi.org/10.1002/stc.2302>
- Ok SY, Kim DS, Park KS, Koh HM (2007) Semi-active fuzzy control of cable-stayed bridges using magneto-rheological dampers. *Eng Struct* 29:776–788. <https://doi.org/10.1016/j.engstruct.2006.06.020>
- Pei P, Peng Y, Qiu C (2021) Magnetorheological damper modeling based on a refined constitutive model for MR fluids. *J Intell Mater Syst Struct*. <https://doi.org/10.1177/1045389X211048231>
- Peng Y, Ma Y, Huang T, De Domenico D (2021a) Reliability-based design optimization of adaptive sliding base isolation system for



- improving seismic performance of structures. *Reliab Eng Syst Saf*. <https://doi.org/10.1016/j.ress.2020.107167>
- Peng Y, Zhou T, Li J (2021b) Surrogate modeling immersed probability density evolution method for structural reliability analysis in high dimensions. *Mech Syst Signal Process*. <https://doi.org/10.1016/j.ymssp.2020.107366>
- Peng Y, Li J (2019) *Stochastic optimal control of structures*. Springer, New York
- Pohoryles DA, Duffour P (2015) Adaptive control of structures under dynamic excitation using magnetorheological dampers: an improved clipped-optimal control algorithm. *J Vib Control* 21:2569–2582. <https://doi.org/10.1177/1077546313510543>
- Shook D, Roschke P, Ozbulut O (2008a) Superelastic semi-active damping of a base-isolated structure. *Struct Control Health Monit* 15:746–768
- Shook DA, Roschke PN, Lin PY, Loh CH (2008b) GA-optimized fuzzy logic control of a large-scale building for seismic loads. *Eng Struct* 30:436–449. <https://doi.org/10.1016/j.engstruct.2007.04.008>
- Shook DA, Roschke PN, Lin P-Y, Loh C-H (2009) Semi-active control of a torsionally-responsive structure. *Eng Struct* 31:57–68
- Spencer BF, Dyke SJ, Sain MK, Carlson JD (1997) Phenomenological model for magnetorheological dampers. *J Eng Mech ASCE* 123:230–238. [https://doi.org/10.1061/\(asce\)0733-9399\(1997\)123:3\(230\)](https://doi.org/10.1061/(asce)0733-9399(1997)123:3(230))
- Teng T-L, Peng C-P, Chuang C (2000) A study on the application of fuzzy theory to structural active control. *Comput Methods Appl Mech Eng* 189:439–448
- Uz ME, Hadi MNS (2014) Optimal design of semi active control for adjacent buildings connected by MR damper based on integrated fuzzy logic and multi-objective genetic algorithm. *Eng Struct* 69:135–148. <https://doi.org/10.1016/j.engstruct.2014.03.006>
- Xu ZD, Xu YW, Wang C, Zhao YL, Ji BH, Du YL (2021) Force tracking model and experimental verification on a novel magnetorheological damper with combined compensator for stay cables of bridge. *Structures* 32:1971–1985. <https://doi.org/10.1016/j.istruc.2021.04.010>
- Yan G, Zhou LL (2006) Integrated fuzzy logic and genetic algorithms for multi-objective control of structures using MR dampers. *J Sound Vib* 296:368–382. <https://doi.org/10.1016/j.jsv.2006.03.011>
- Yang G (2001) Large-scale magnetorheological fluid damper for vibration mitigation: modeling, testing and control. *Dissertation Abstracts International*, Volume: 62–10, Section: B, page: 4674; Director: B F Spence
- Yoshida O, Dyke SJ (2004) Seismic control of a nonlinear benchmark building using smart dampers. *J Eng Mech* 130:386–392. [https://doi.org/10.1061/\(ASCE\)0733-9399\(2004\)130:4\(386\)](https://doi.org/10.1061/(ASCE)0733-9399(2004)130:4(386))
- Yuen KV, Shi Y, Beck JL, Lam HF (2007) Structural protection using MR dampers with clipped robust reliability-based control. *Struct Multidisc Optim* 34:431–443. <https://doi.org/10.1007/s00158-007-0097-3>
- Zafarani MM, Halabian AM, Behbahani S (2018) Optimal coupled and uncoupled fuzzy logic control for magneto-rheological damper-equipped plan-asymmetric structural systems considering structural nonlinearities. *J Vib Control* 24:1364–1390. <https://doi.org/10.1177/1077546316660030>
- Zhang Z, Peng Y (2020) Dynamic physical model for MR damper considering chain deflection in preyield stage. *J Eng Mech* 146:04020122
- Zhao YL, Xu ZD, Wang C (2019) Wind vibration control of stay cables using magnetorheological dampers under optimal equivalent control algorithm. *J Sound Vib* 443:732–747. <https://doi.org/10.1016/j.jsv.2018.12.016>

**Publisher's Note** Springer Nature remains neutral with regard to jurisdictional claims in published maps and institutional affiliations.

Springer Nature or its licensor holds exclusive rights to this article under a publishing agreement with the author(s) or other rightsholder(s); author self-archiving of the accepted manuscript version of this article is solely governed by the terms of such publishing agreement and applicable law.